Some New Three-Dimensional Green's Functions in Anisotropic Piezoelectric Bimaterials

E. Pan
Dept. of Civil Engineering
The University of Akron
Akron, OH 44325-3905

Abstract

In this paper, we derive three-dimensional Green's functions of point-force/point-charge in anisotropic and piezoelectric bimaterials for six different interface models. Mechanically, the six interface models are either in perfect or smooth contact along the interface; electronically, they can be closed, open interface, or with continuous electrical potential and normal electrical displacement component along the interface. By introducing certain modified bimaterial Stroh matrices, along with the extended Stroh formalism and the Mindlin's superposition method, the bimaterial Green's functions for the six interface conditions are expressed in terms of a concise and mathematically similar uniform form. That is, the physical-domain bimaterial Green's functions can all be expressed as a sum of a homogeneous full-space Green's function in an explicit form and a complementary part in terms of simple line-integrals over $[0, \pi]$ suitable for standard numerical integration. Furthermore, utilizing a direct connection between the 2D and 3D Stroh matrices observed in this paper, the corresponding 2D bimaterial Green's functions are also derived, in exact-closed form, for the six interface conditions.

Based on the bimaterial Green's functions, the effects of different interface conditions on the mechanical and electrical fields are discussed. It is noted that only the complementary part of the solution contributes to the differences of the mechanical and electrical fields arising from different interface conditions. Also, numerical examples are presented for the Green's functions in the bimaterials made of two half-spaces with two typical piezoelectric materials, quartz and ceramic. Certain new features are observed which could be of great interest to the design of piezoelectric composites and to the numerical modeling of strained quantum devices using the boundary element method.

1. Introduction

Green's functions in anisotropic and fully coupled piezoelectric solids are of great importance in the analyses of micromechanical devices (Yang and Tiersten 1997; Fang et al., 2001), composite structures (Suo et al., 1992; Dunn and Taya, 1993; Ting, 1996, 2000, 2001), and certain generalized Hertzian contact problems (Willis, 1966; Fan et al, 1996; Chen, 1999; Chen et al., 1999). More importantly, piezoelectric Green's functions are required in the boundary integral equation method for the modeling of piezoelectric structures (Pan, 1999; Denda and Lua, 1999; Liu and Fan, 2001; Davi and Milazzo, 2002).

In recent years, both two-dimensional (2D) and three-dimensional (3D) Green's functions and related analytical methods have been developed for, and applied particularly to, the study of the strain-induced semiconductor quantum structures where

the quantum wire/dot growth directly effects the electronic and optical performance (see, e.g., Andreev et al., 1999; Davies, 1998, 1999; Davies and Larkin, 1994; Faux and Pearson, 2000; Faux et al., 1996, 1997; Freund, 2000; Freund and Gosling, 1995; Gosling and Willis, 1994, 1995; Larkin et al., 1997; Holy et al. 1999; Park and Chuang, 1998; Pearson and Faux, 2000; Hearne et al., 2000; Romanov et al. 2001; Einfeldt et al., 2001). Even with a purely elastic model or certain semi-coupled piezoelectric models, some interesting results have been found on the effect of crystal anisotropy (Faux and Pearson, 2000), on the relations between the elastic field and the orientation and ordering of the quantum dot and superlattice growth (Grundmann et al., 1995; Davies, 1998, 1999; Holy et al. 1999), and on the piezoelectric effect (Grundmann et al., 1995; Davies, 1998, 1999). It is apparent that a fully coupled anisotropic and piezoelectric model would be more reliable should a numerical modeling result be applied to the design process in the semiconductor devices. Such a numerical study, however, requires the fully coupled piezoelectric Green's function, which unfortunately, poses great difficulties due to the crystal anisotropy and piezoelectric coupling. Recently, Ru (2001) solved the Eshelby's problem in a piezoelectric bimaterial plane with fully coupled constitutive relation, and the author (Pan, 2002a) derived the generalized Mindlin solution in an anisotropic and piezoelectric half-space with general boundary conditions on the surface. Ru's (2001) analytical solutions and Pan's (2002a) numerical results have both clearly indicated the effect of different piezoelectric boundary conditions on the surface response of both mechanical and electrical quantities. Therefore, these fully coupled 2D and 3D solutions provide the mathematical formulation that can be applied to the analysis of the strained quantum dot growth and other related problems. Actually, the author has been able to apply successfully the generalized Mindlin solution (Pan, 2002a) to calculate the quantum dot induced elastic and piezoelectric fields in certain semiconductor substrates and to show the importance of the fully coupled piezoelectric model in this application (Pan, 2002b).

Besides the piezoelectric coupling effect, self-assembled quantum-dot structures are inherently heterogeneous; in particular, they are often in multilayered structures (see, for example, Lee et al., 2001; Yeh et al., 2000). A multilayered structure, with different crystal material and interface conditions, will affect the nucleation, ordering, and positioning of the quantum dots, and consequently the electronic and optical properties of the devices (Grundmann et al., 1995; Holy et al., 1999; Lee et al., 2000; Yang et al., 2000; Yeh et al., 2000; Kim et al., 2001; Lee et al., 2001). Unfortunately, in such a complicated structure, the Green's function solution in either a homogeneous infinite-space or half-space is unsuitable. A bimaterial model with suitable interface conditions is needed in order to capture the elastic and electric behavior near the interface. While several imperfect interface models have been developed for, and applied to, various engineering and physical problems associated with purely elastic bimaterial structures (see, e.g., Dundurs and Hetenyi, 1965; Benveniste, 1984; Hashin, 1990, 1991; Pagano and Tandon, 1990; Gharpuray et al., 1991; Kouris, 1993; Ru, 1998; Yu, 1998; Shilkrot and Srolovitz, 1998; Benveniste, 1999; Shuvalov and Gorkunova, 1999; Benveniste and Chen, 2001; Hashin, 2001), there is nearly no literature available on the corresponding piezoelectric bimaterials with imperfect interface conditions. The only relevant work is by Abbudi and Barnett (1990) and Alshits et al. (1994) where they studied the interface wave between two anistropic and piezoelectric solids with six different interface

conditions. Specifically, they addressed the existence problem on the localized acoustic wave on the interface when the six different interface conditions are assumed (Alshits et al., 1994).

In this paper, we derive analytically the 3D Green's function of point-force/point-charge in anisotropic and piezoelectric bimaterials with six different interface models. In the six interface models, as in Abbudi and Barnett (1990) and Alshits et al. (1994), the mechanical condition is either perfect-bond or smooth-bond; electrically, the interface can be open, closed, or with continuous electrical potential and normal electrical displacement component. This bimaterial Green's function for the six interface models is obtained uniformly by introducing the modified bimaterial Stroh matrices $\boldsymbol{A}$, $\boldsymbol{B}$, and $\boldsymbol{M}$ (to be defined latter) and by applying the 2D Fourier transforms in combination with Mindlin's superposition method. More specifically, it is expressed as a sum of the infinite-space Green's function and a complementary part. While the former is in an explicit form, as previously derived by Pan and Tonon (2000), the latter is expressed in terms of a simple line integral over $[0, \pi]$. With the exception of the bimaterial Green's function for the perfect-bond interface (Ding et al., 1997; Dunn and Wienecke, 1999; Pan and Yuan, 2000), the Green's function solutions with other five (imperfect) interface models are presented *for the first time*. We also remark that the present methodology can be employed to find the bimaterial Green's functions corresponding to many other interface models. Furthermore, a direct connection between the 2D and 3D Stroh matrices (Ting, 1996) is also observed and thus used to derive the 2D bimaterial Green's functions (in the exact-closed form) for the six different interface models.

The effect of different interface conditions on the mechanical and electrical quantities is then studied. To illustrate the significance of different interface models as well as the electromechanical coupling in the analysis of the piezoelectric problem, numerical examples are carried out for two bimaterial systems made of two typical piezoelectric materials, namely, the quartz with weak coupling and ceramic with strong coupling. Depending upon the source type (mechanical or electrical point source) and source location (in quartz or ceramic half-space), various interesting new features are observed which could be of great interest in the design of piezoelectric composites, in the study of the 3D Eshelby's problem (Eshelby, 1957; Mura, 1987), and in the numerical modeling of strained quantum devices based on the 2D and 3D bimaterial Green's function methods.

This paper is organized as follows: In section 2, the bimaterial Green's function problem is defined along with the mathematical equations and the six different interface models. In section 3, we derive the general solution in the Fourier-transformed domain by introducing certain modified Stroh matrices. While in section 4 the physical-domain bimaterial Green's solution is presented, the effect of different interface conditions on the mechanical and electrical fields is studied in section 5. Numerical examples are given in section 6, and certain conclusions are drawn in section 7, along with a brief discussion on how the present analytical bimaterial Green's functions can be applied to 2D quantum wire and 3D quantum dot analyses. Throughout this paper, by Green's functions, we mean the elastic displacements and electrical potential, elastic stresses and electrical displacements, and derivatives of them with respect to the source coordinates.

2. Description of the Generalized Bimaterial Problem

Consider an anisotropic and piezoelectric bimaterial full-space where $x_3 > 0$ and $x_3 < 0$ are occupied by materials 1 and 2, respectively (Figure 1), with interface being at $x_3 = 0$ plane. Without loss of generality, we assume that an extended point force $\boldsymbol{f} = (f_1, f_2, f_3, -q)^t$ is applied in material 1 at source point $\boldsymbol{d} \equiv (d_1, d_2, d_3 \equiv d > 0)$, with the field point being denoted by $\boldsymbol{x} \equiv (x_1, x_2, x_3 \equiv z)$ [*]. Following Pan and Yuan (2000), we artificially divide the problem domain into three regions: $z > d$ (in material 1), $0 \le z < d$ (in material 1), and $z < 0$ (in material 2). Within each region, the equilibrium equation and constitutive law can be written, in terms of a shorthand notation (see, Barnett and Lothe, 1975; Pan, 1999), as

$$\sigma_{iJ,i} = 0 \tag{2.1}$$

$$\sigma_{iJ} = C_{iJKl}\gamma_{Kl} \tag{2.2}$$

In equation (2.1) and (2.2), lowercase (uppercase) subscripts take the range from 1 to 3 (1 to 4), and summation over repeated subscripts is implied.

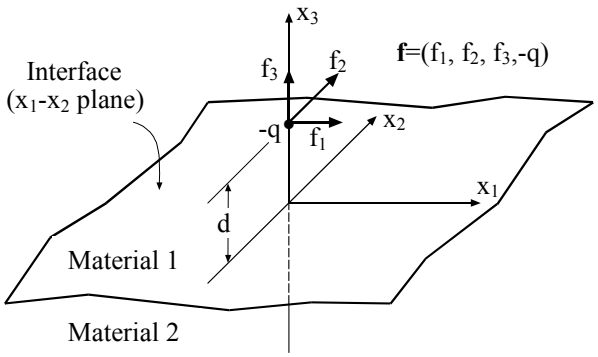

Figure 1. An anisotropic piezoelectric bimaterial full-space subjected to an extended concentrated force $\boldsymbol{f}$ applied at point (0,0,d>0) in material 1 under 3D deformation. Under 2D deformation in the (x_1,x_3)- or (x,z)-plane, the extended force $\boldsymbol{f}$ and also an extended dislocation $\boldsymbol{b}$ are applied along the line in the x_2-direction, which intercepts the (x_1,x_3)-plane at (0,d>0) in material 1.

The extended field quantities, including the displacement, strain, stress, and stiffness matrix, are defined as (Barnett and Lothe, 1975; Dunn and Taya, 1993; Pan, 1999)

$$u_I = \begin{cases} u_i, & I = 1, 2, 3 \\ \phi, & I = 4 \end{cases} \tag{2.3}$$

[*] Thereafter, the scalar variables z and d will be used exclusively for the third field and source coordinates x_3 and d_3, respectively.

$$\gamma_{Ij} = \begin{cases} \gamma_{ij} = 0.5(u_{j,i} + u_{i,j}), & I = 1, 2, 3 \\ -E_j = \phi_{,j}, & I = 4 \end{cases} \tag{2.4}$$

$$\sigma_{iJ} = \begin{cases} \sigma_{ij}, & J = 1, 2, 3 \\ D_i, & J = 4 \end{cases} \tag{2.5}$$

$$C_{iJKl} = \begin{cases} C_{ijkl}, & J, K = 1, 2, 3 \\ e_{lij}, & J = 1, 2, 3; \ K = 4 \\ e_{ikl}, & J = 4; \ K = 1, 2, 3 \\ -\varepsilon_{il}, & J = K = 4 \end{cases} \tag{2.6}$$

In equations (2.3)-(2.6), u_i and ϕ are the elastic displacement and electrical potential, respectively; γ_{ij} is the elastic strain and E_i the electrical field; C_{ijlm}, e_{ijk}, and ε_{ij} are the elastic moduli, the piezoelectric coefficients, and the dielectric constants, respectively. We remark that while these coefficients are required to satisfy the well-known symmetry conditions (Pan, 1999), the decoupled state (purely elastic and purely electrical deformations) can be obtained by simply setting $e_{ijk} = 0$. This decoupled state and other semi-coupled approaches were adopted in most previous studies in strained quantum devices.

In the following sections, we will also use *the extended displacement* for the elastic displacement and electrical potential as defined by (2.3), *the extended stress* for the stress and electrical displacement as defined by (2.5), and *the extended stiffness matrix* for all the material constants as defined by (2.6). Furthermore, the *extended* traction and in-plane stress vectors defined as below will be also used in the paper:

$$\begin{aligned} \boldsymbol{t} &= (t_1, \ t_2, \ t_3, \ t_4)^t \equiv (\sigma_{31}, \ \sigma_{32}, \ \sigma_{33}, \ D_3)^t \\ \boldsymbol{s} &= (s_1, \ s_2, \ s_3, \ s_4, \ s_5)^t \equiv (\sigma_{11}, \ \sigma_{12}, \ \sigma_{22}, \ D_1, \ D_2)^t \end{aligned} \tag{2.7a,b}$$

To solve equations (2.1) and (2.2), a suitable interface condition and the condition across the source level need to be described. In this paper, we will restrict ourselves to the following six interface models, although more general interface conditions can be considered.

Model 1: The extended displacement and traction vectors are continuous across the interface, i.e.,

$$u_J^{(1)}\Big|_{z=0^+} = u_J^{(2)}\Big|_{z=0^-}, \quad t_J^{(1)}\Big|_{z=0^+} = t_J^{(2)}\Big|_{z=0^-}; \ J = 1,2,3,4 \tag{2.8}$$

This is, perhaps, the most frequently studied interface model in piezoelectric bimaterial system. Recently, Pan and Yuan (2000) derived the corresponding bimaterial Green's functions using the extended Stroh formalism and the Mindlin's superposition method. In the following discussion, this model will be named as the perfect-bond interface model, while the other five models will be called imperfect interface models for simplicity.

Model 2: The mechanical displacement and traction vectors are continuous across the interface, and the electrical potential is zero along the interface, i.e.,

$$\begin{aligned} &u_j^{(1)}\Big|_{z=0^+} = u_j^{(2)}\Big|_{z=0^-}, \quad t_j^{(1)}\Big|_{z=0^+} = t_j^{(2)}\Big|_{z=0^-}; \ j = 1,2,3 \\ &u_4^{(1)}\Big|_{z=0^+} = u_4^{(2)}\Big|_{z=0^-} = 0 \end{aligned} \tag{2.9}$$

It is seen that this interface is electrically closed (Alshits et al., 1994) or it is an electrical wall, and is a very common case in electromagnetic studies (see, Papas, 1988 or Volakis et al., 1998). Furthermore, for advanced composites which are made of piezoelectric and purely elastic but ideal conductive materials, the interface condition between the piezoelectric and elastic ideal conductor is model 2 where the electric potential along the interface is zero. Very recently, Tevaarwerk et al. (2002) studied electrically isolated quantum dots and argued that such special quantum dots are promising candidates for charge storage in future silicon nanoelectronics. The electrically isolated SiGe QDs are grown on ultrathin silicon-on-insulator where the thin layer of silicon acts as a conductor which could be approximated with the interface model 2. The metal-insulator-semiconductor (MIS) structures have been long used in semiconductor industry for high performance field-effect transistors (see, e.g., Reed et al, 1994) where the interfaces between metal/insulator and insulator/semiconductor need to be modeled suitably, perhaps with the interface model 2 as one of the choices in the approximation.

Model 3: The mechanical displacement and traction vectors are continuous across the interface, and the normal electrical displacement is zero along the interface, i.e.,

$$\begin{aligned} &u_j^{(1)}\Big|_{z=0^+} = u_j^{(2)}\Big|_{z=0^-}, \quad t_j^{(1)}\Big|_{z=0^+} = t_j^{(2)}\Big|_{z=0^-}; \; j = 1,2,3 \\ &t_4^{(1)}\Big|_{z=0^+} = t_4^{(2)}\Big|_{z=0^-} = 0 \end{aligned} \tag{2.10}$$

Similarly, this interface is electrically open (Alshits et al., 1994) or it is a magnetic wall, and is again a very common case in electromagnetic studies (see, Papas, 1988 or Volakis et al., 1998).

In these three models, the mechanical displacement and traction vectors are assumed to be continuous across the interface, corresponding to the purely elastic bimaterials with perfect-bond interface condition. In the following three models, the mechanical perfect-bond condition is replaced by the mechanical smooth-bond condition.

Model 4: Across the interface, the mechanical displacement and traction vectors are in smooth contact, and the electrical potential and normal electrical displacement component are continuous:

$$\begin{aligned} &u_m^{(1)}\Big|_{z=0^+} = u_m^{(2)}\Big|_{z=0^-}, \quad t_m^{(1)}\Big|_{z=0^+} = t_m^{(2)}\Big|_{z=0^-}; \; m = 3,4 \\ &t_\alpha^{(1)}\Big|_{z=0^+} = t_\alpha^{(2)}\Big|_{z=0^-} = 0, \; \alpha = 1,2 \end{aligned} \tag{2.11}$$

Model 5: Across the interface the mechanical displacement and traction vectors are in smooth contact, and along the interface the electrical potential is zero:

$$\begin{aligned} &u_3^{(1)}\Big|_{z=0^+} = u_3^{(2)}\Big|_{z=0^-}, \quad t_3^{(1)}\Big|_{z=0^+} = t_3^{(2)}\Big|_{z=0^-} \\ &t_\alpha^{(1)}\Big|_{z=0^+} = t_\alpha^{(2)}\Big|_{z=0^-} = 0 \; ; \alpha = 1,2 \\ &u_4^{(1)}\Big|_{z=0^+} = u_4^{(2)}\Big|_{z=0^-} = 0 \end{aligned} \tag{2.12}$$

We remark that models 4 and 5 are important in describing the connection between two materials at elevated temperature (Shilkrot and Srolovitz, 1998) and in modeling the bone implants in biomechanics (Gharpuray et al., 1991).

Model 6: Across the interface the mechanical displacement and traction vectors are in smooth contact, and along the interface the normal electrical displacement component is zero:

$$\begin{aligned} & u_3^{(1)}\Big|_{z=0^+} = u_3^{(2)}\Big|_{z=0^-}, \quad t_3^{(1)}\Big|_{z=0^+} = t_3^{(2)}\Big|_{z=0^-} \\ & t_\alpha^{(1)}\Big|_{z=0^+} = t_\alpha^{(2)}\Big|_{z=0^-} = 0 \; ; \alpha = 1,2 \\ & t_4^{(1)}\Big|_{z=0^+} = t_4^{(2)}\Big|_{z=0^-} = 0 \end{aligned} \tag{2.13}$$

When an extended point force $\boldsymbol{f} = (f_1, f_2, f_3, f_4)^t$ is applied in the piezoelectric bimaterials at the source point $\boldsymbol{d} \equiv (d_1, d_2, d_3 \equiv d)$ with $d_3 > 0$, the extended displacement and traction vectors are required to satisfy the following conditions (using vector $\boldsymbol{u}$ for the extended displacement and vector $\boldsymbol{t}$ for the extended traction, each with four components)

$$\begin{aligned} & \boldsymbol{u}\Big|_{z=d^-} = \boldsymbol{u}\Big|_{z=d^+} \\ & \boldsymbol{t}\Big|_{z=d^-} - \boldsymbol{t}\Big|_{z=d^+} = \delta(x_1 - d_1)\delta(x_2 - d_2)\boldsymbol{f} \end{aligned} \tag{2.14}$$

In summary, therefore, the bimaterial Green's function problem is to find the mechanical and electrical fields that satisfy (2.1) for the three regions $z > d$, $0 \le z < d$, and $z < 0$, one of the interface conditions (2.8)-(2.13), the conditions (2.14) at the source level, along with the radiation condition so that the solution in the bimaterial full-space vanishes as $|\boldsymbol{x}|$ approaches infinity.

3. Stroh Formalism and Solution in the Transformed Domain

Similar to the anisotropic and piezoelectric bimaterial case with interface Model 1 (i.e, the perfect-bond interface), we first apply the 2D Fourier transforms to the problem equations to express the Fourier transformed general solutions in terms of the extended Stroh formalism (Ting, 1996; Pan and Yuan, 2000). We then introduce the modified bimaterial Stroh matrices in order to find the Fourier transformed bimaterial Green's functions. This is described below.

First, the 2D Fourier transforms (i.e., for the two-point extended displacement)

$$\widetilde{u}_K(y_1, y_2, z; \boldsymbol{d}) = \iint u_K(x_1, x_2, z; \boldsymbol{d}) e^{iy_\alpha x_\alpha} dx_1 dx_2 \tag{3.1}$$

are applied to equations (2.1), (2.2), and (2.4). In (3.1), α takes the summation from 1 to 2. We add that, when carrying out the double Fourier inverse transforms later on, a polar coordinate transform that relates the Fourier variables (y_1, y_2), defined below as

$$y_1 = \eta \cos\theta \; ; \; y_2 = \eta \sin\theta \tag{3.2}$$

will be used.

Then, the general solutions in the Fourier transformed domain, which satisfy condition (2.14) at the source level and the radiation condition as $|\boldsymbol{x}|$ approaches infinity, can be derived as (Ting, 1996; Pan and Yuan, 2000)

For $z > d$ (in material 1):

$$\begin{aligned}
\widetilde{\boldsymbol{u}}^{(1)}(y_1,y_2,z;\boldsymbol{d}) &= -i\eta^{-1}\overline{\boldsymbol{A}}^{(1)}\langle e^{-i\overline{p}_*^{(1)}\eta(z-d)}\rangle\overline{\boldsymbol{q}}^{\infty} - i\eta^{-1}\overline{\boldsymbol{A}}^{(1)}\langle e^{-i\overline{p}_*^{(1)}\eta z}\rangle\overline{\boldsymbol{q}}^{(1)} \\
\widetilde{\boldsymbol{t}}^{(1)}(y_1,y_2,z;\boldsymbol{d}) &= -\overline{\boldsymbol{B}}^{(1)}\langle e^{-i\overline{p}_*^{(1)}\eta(z-d)}\rangle\overline{\boldsymbol{q}}^{\infty} - \overline{\boldsymbol{B}}^{(1)}\langle e^{-i\overline{p}_*^{(1)}\eta z}\rangle\overline{\boldsymbol{q}}^{(1)} \\
\widetilde{\boldsymbol{s}}^{(1)}(y_1,y_2,z;\boldsymbol{d}) &= -\overline{\boldsymbol{C}}^{(1)}\langle e^{-i\overline{p}_*^{(1)}\eta(z-d)}\rangle\overline{\boldsymbol{q}}^{\infty} - \overline{\boldsymbol{C}}^{(1)}\langle e^{-i\overline{p}_*^{(1)}\eta z}\rangle\overline{\boldsymbol{q}}^{(1)}
\end{aligned} \tag{3.3}$$

For $0 \le z < d$ (in material 1):

$$\begin{aligned}
\widetilde{\boldsymbol{u}}^{(1)}(y_1,y_2,z;\boldsymbol{d}) &= i\eta^{-1}\boldsymbol{A}^{(1)}\langle e^{-ip_*^{(1)}\eta(z-d)}\rangle\boldsymbol{q}^{\infty} - i\eta^{-1}\overline{\boldsymbol{A}}^{(1)}\langle e^{-i\overline{p}_*^{(1)}\eta z}\rangle\overline{\boldsymbol{q}}^{(1)} \\
\widetilde{\boldsymbol{t}}^{(1)}(y_1,y_2,z;\boldsymbol{d}) &= \boldsymbol{B}^{(1)}\langle e^{-ip_*^{(1)}\eta(z-d)}\rangle\boldsymbol{q}^{\infty} - \overline{\boldsymbol{B}}^{(1)}\langle e^{-i\overline{p}_*^{(1)}\eta z}\rangle\overline{\boldsymbol{q}}^{(1)} \\
\widetilde{\boldsymbol{s}}^{(1)}(y_1,y_2,z;\boldsymbol{d}) &= \boldsymbol{C}^{(1)}\langle e^{-ip_*^{(1)}\eta(z-d)}\rangle\boldsymbol{q}^{\infty} - \overline{\boldsymbol{C}}^{(1)}\langle e^{-i\overline{p}_*^{(1)}\eta z}\rangle\overline{\boldsymbol{q}}^{(1)}
\end{aligned} \tag{3.4}$$

For $z < 0$ (in material 2):

$$\begin{aligned}
\widetilde{\boldsymbol{u}}^{(2)}(y_1,y_2,z;\boldsymbol{d}) &= i\eta^{-1}\boldsymbol{A}^{(2)}\langle e^{-ip_*^{(2)}\eta z}\rangle\boldsymbol{q}^{(2)} \\
\widetilde{\boldsymbol{t}}^{(2)}(y_1,y_2,z;\boldsymbol{d}) &= \boldsymbol{B}^{(2)}\langle e^{-ip_*^{(2)}\eta z}\rangle\boldsymbol{q}^{(2)} \\
\widetilde{\boldsymbol{s}}^{(2)}(y_1,y_2,z;\boldsymbol{d}) &= \boldsymbol{C}^{(2)}\langle e^{-ip_*^{(2)}\eta z}\rangle\boldsymbol{q}^{(2)}
\end{aligned} \tag{3.5}$$

where

$$\langle e^{-ip_*\eta z}\rangle = diag[e^{-ip_1\eta z},\quad e^{-ip_2\eta z},\quad e^{-ip_3\eta z},\ e^{-ip_4\eta z}] \tag{3.6}$$

and

$$\boldsymbol{q}^{\infty} = (\boldsymbol{A}^{(1)})^T\boldsymbol{f}e^{iy_\alpha d_\alpha}\ ;\ \overline{\boldsymbol{q}}^{\infty} = (\overline{\boldsymbol{A}}^{(1)})^T\boldsymbol{f}e^{iy_\alpha d_\alpha} \tag{3.7a,b}$$

In equations (3.3)-(3.5), p_J (J=1,2,3,4), and $\boldsymbol{A}$, $\boldsymbol{B}$, and $\boldsymbol{C}$ are the Stroh eigenvalues and eigenmatrices, and their expressions can be found in Pan and Yuan (2000) or Pan (2002a). Also in equations (3.3)-(3.5), η is the Fourier radial variable defined by equation (3.2).

The complex vectors $\overline{\boldsymbol{q}}^{(1)}$ and $\boldsymbol{q}^{(2)}$ in equations (3.3)-(3.5) are to be determined by the interface conditions. While these two complex vectors are different for different interface conditions, a concise and unified expression can be derived for them by introducing certain modified Stroh matrices. This procedure is illustrated below for the six different interface models.

Model 1: For the perfect-bond interface Model 1, it is found that the complex vectors $\overline{\boldsymbol{q}}^{(1)}$ and $\boldsymbol{q}^{(2)}$ are required to satisfy the following two vector conditions (Ting, 1996; Pan and Yuan, 2000)

$$\boldsymbol{A}^{(1)}\langle e^{ip_*^{(1)}\eta d}\rangle\boldsymbol{q}^{\infty} - \overline{\boldsymbol{A}}^{(1)}\overline{\boldsymbol{q}}^{(1)} = \boldsymbol{A}^{(2)}\boldsymbol{q}^{(2)} \tag{3.8a}$$

$$\boldsymbol{B}^{(1)}\langle e^{ip_*^{(1)}\eta d}\rangle\boldsymbol{q}^{\infty} - \overline{\boldsymbol{B}}^{(1)}\overline{\boldsymbol{q}}^{(1)} = \boldsymbol{B}^{(2)}\boldsymbol{q}^{(2)} \tag{3.8b}$$

Model 2: For this interface model, the continuity conditions of the mechanical displacement and traction vectors across the interface and the condition that the electrical potential is zero on the interface give the following interface equations from which the complex vectors $\overline{\boldsymbol{q}}^{(1)}$ and $\boldsymbol{q}^{(2)}$ are to be solved:

$$\begin{pmatrix} A_{11}^{(1)} & A_{12}^{(1)} & A_{13}^{(1)} & A_{14}^{(1)} \\ A_{21}^{(1)} & A_{22}^{(1)} & A_{23}^{(1)} & A_{24}^{(1)} \\ A_{31}^{(1)} & A_{32}^{(1)} & A_{33}^{(1)} & A_{34}^{(1)} \end{pmatrix} \langle e^{ip_*^{(1)}\eta d} \rangle \boldsymbol{q}^{\infty} - \begin{pmatrix} \overline{A}_{11}^{(1)} & \overline{A}_{12}^{(1)} & \overline{A}_{13}^{(1)} & \overline{A}_{14}^{(1)} \\ \overline{A}_{21}^{(1)} & \overline{A}_{22}^{(1)} & \overline{A}_{23}^{(1)} & \overline{A}_{24}^{(1)} \\ \overline{A}_{31}^{(1)} & \overline{A}_{32}^{(1)} & \overline{A}_{33}^{(1)} & \overline{A}_{34}^{(1)} \end{pmatrix} \overline{\boldsymbol{q}}^{(1)} = \begin{pmatrix} A_{11}^{(2)} & A_{12}^{(2)} & A_{13}^{(2)} & A_{14}^{(2)} \\ A_{21}^{(2)} & A_{22}^{(2)} & A_{23}^{(2)} & A_{24}^{(2)} \\ A_{31}^{(2)} & A_{32}^{(2)} & A_{33}^{(2)} & A_{34}^{(2)} \end{pmatrix} \boldsymbol{q}^{(2)} \tag{3.9a}$$

$$\begin{pmatrix} B_{11}^{(1)} & B_{12}^{(1)} & B_{13}^{(1)} & B_{14}^{(1)} \\ B_{21}^{(1)} & B_{22}^{(1)} & B_{23}^{(1)} & B_{24}^{(1)} \\ B_{31}^{(1)} & B_{32}^{(1)} & B_{33}^{(1)} & B_{34}^{(1)} \end{pmatrix} \langle e^{ip_*^{(1)}\eta d} \rangle \boldsymbol{q}^{\infty} - \begin{pmatrix} \overline{B}_{11}^{(1)} & \overline{B}_{12}^{(1)} & \overline{B}_{13}^{(1)} & \overline{B}_{14}^{(1)} \\ \overline{B}_{21}^{(1)} & \overline{B}_{22}^{(1)} & \overline{B}_{23}^{(1)} & \overline{B}_{24}^{(1)} \\ \overline{B}_{31}^{(1)} & \overline{B}_{32}^{(1)} & \overline{B}_{33}^{(1)} & \overline{B}_{34}^{(1)} \end{pmatrix} \overline{\boldsymbol{q}}^{(1)} = \begin{pmatrix} B_{11}^{(2)} & B_{12}^{(2)} & B_{13}^{(2)} & B_{14}^{(2)} \\ B_{21}^{(2)} & B_{22}^{(2)} & B_{23}^{(2)} & B_{24}^{(2)} \\ B_{31}^{(2)} & B_{32}^{(2)} & B_{33}^{(2)} & B_{34}^{(2)} \end{pmatrix} \boldsymbol{q}^{(2)} \tag{3.9b}$$

$$\begin{pmatrix} A_{41}^{(1)} & A_{42}^{(1)} & A_{43}^{(1)} & A_{44}^{(1)} \end{pmatrix} \langle e^{ip_*^{(1)}\eta d} \rangle \boldsymbol{q}^{\infty} - \begin{pmatrix} \overline{A}_{41}^{(1)} & \overline{A}_{42}^{(1)} & \overline{A}_{43}^{(1)} & \overline{A}_{44}^{(1)} \end{pmatrix} \overline{\boldsymbol{q}}^{(1)} = 0 \tag{3.9c}$$

$$\begin{pmatrix} A_{41}^{(2)} & A_{42}^{(2)} & A_{43}^{(2)} & A_{44}^{(2)} \end{pmatrix} \boldsymbol{q}^{(2)} = 0 \tag{3.9d}$$

It is seen that it would be very complicated if one solves directly these equations for the complex vectors $\overline{\boldsymbol{q}}^{(1)}$ and $\boldsymbol{q}^{(2)}$. However, by some simple additions and subtractions, these equations can be grouped into two matrix equations that are equivalent to the above. In this way, we found that:

$$\boldsymbol{A}^{(1)} \langle e^{ip_*^{(1)}\eta d} \rangle \boldsymbol{q}^{\infty} - \overline{\boldsymbol{A}}^{(1)} \overline{\boldsymbol{q}}^{(1)} = \boldsymbol{A}^{(2)} \boldsymbol{q}^{(2)} \tag{3.10a}$$

$$\begin{pmatrix} B_{11}^{(1)} & B_{12}^{(1)} & B_{13}^{(1)} & B_{14}^{(1)} \\ B_{21}^{(1)} & B_{22}^{(1)} & B_{23}^{(1)} & B_{24}^{(1)} \\ B_{31}^{(1)} & B_{32}^{(1)} & B_{32}^{(1)} & B_{34}^{(1)} \\ A_{41}^{(1)} & A_{42}^{(1)} & A_{43}^{(1)} & A_{44}^{(1)} \end{pmatrix} \langle e^{ip_*^{(1)}\eta d} \rangle \boldsymbol{q}^{\infty} - \begin{pmatrix} \overline{B}_{11}^{(1)} & \overline{B}_{12}^{(1)} & \overline{B}_{13}^{(1)} & \overline{B}_{14}^{(1)} \\ \overline{B}_{21}^{(1)} & \overline{B}_{22}^{(1)} & \overline{B}_{23}^{(1)} & \overline{B}_{24}^{(1)} \\ \overline{B}_{31}^{(1)} & \overline{B}_{32}^{(1)} & \overline{B}_{32}^{(1)} & \overline{B}_{34}^{(1)} \\ \overline{A}_{41}^{(1)} & \overline{A}_{42}^{(1)} & \overline{A}_{43}^{(1)} & \overline{A}_{44}^{(1)} \end{pmatrix} \overline{\boldsymbol{q}}^{(1)} = \begin{pmatrix} B_{11}^{(2)} & B_{12}^{(2)} & B_{13}^{(2)} & B_{14}^{(2)} \\ B_{21}^{(2)} & B_{22}^{(2)} & B_{23}^{(2)} & B_{24}^{(2)} \\ B_{31}^{(2)} & B_{32}^{(2)} & B_{32}^{(2)} & B_{34}^{(2)} \\ -A_{41}^{(2)} & -A_{42}^{(2)} & -A_{43}^{(2)} & -A_{44}^{(2)} \end{pmatrix} \boldsymbol{q}^{(2)} \tag{3.10b}$$

The structure of this linear system for the complex vectors $\overline{\boldsymbol{q}}^{(1)}$ and $\boldsymbol{q}^{(2)}$ is now similar to that for the interface Model 1 (3.8a,b). Consequently, the solution for the complex vectors $\overline{\boldsymbol{q}}^{(1)}$ and $\boldsymbol{q}^{(2)}$ should also have a similar structure as for the interface Model 1 if certain modified Stroh matrices are introduced. We now derive the exact solution for these two vectors.

We have seen that, for the interface Model 1, the solution for the complex vectors $\overline{\boldsymbol{q}}^{(1)}$ and $\boldsymbol{q}^{(2)}$ has the following simple expression (Pan and Yuan, 2000)

$$\begin{aligned} \overline{\boldsymbol{q}}^{(1)} &= \boldsymbol{G}_1 \langle e^{ip_*^{(1)}\eta d} \rangle \boldsymbol{q}^{\infty} \\ \boldsymbol{q}^{(2)} &= \boldsymbol{G}_2 \langle e^{ip_*^{(1)}\eta d} \rangle \boldsymbol{q}^{\infty} \end{aligned} \tag{3.11}$$

where, the matrices $\boldsymbol{G}_1$ and $\boldsymbol{G}_2$ are given by (Pan and Yuan, 2000)

$$\begin{aligned} \boldsymbol{G}_1 &= -(\overline{\boldsymbol{A}}^{(1)})^{-1} (\overline{\boldsymbol{M}}^{(1)} + \boldsymbol{M}^{(2)})^{-1} (\boldsymbol{M}^{(1)} - \boldsymbol{M}^{(2)}) \boldsymbol{A}^{(1)} \\ \boldsymbol{G}_2 &= (\boldsymbol{A}^{(2)})^{-1} (\overline{\boldsymbol{M}}^{(1)} + \boldsymbol{M}^{(2)})^{-1} (\boldsymbol{M}^{(1)} + \overline{\boldsymbol{M}}^{(1)}) \boldsymbol{A}^{(1)} \end{aligned} \tag{3.12}$$

with $\boldsymbol{M}^{(\alpha)}$ being the impedance tensors defined as

$$\boldsymbol{M}^{(\alpha)} = -i\boldsymbol{B}^{(\alpha)} (\boldsymbol{A}^{(\alpha)})^{-1} \qquad (\alpha = 1, 2) \tag{3.13}$$

It is readily to see that, for the interface Model 2, the solution for the complex vectors $\overline{\boldsymbol{q}}^{(1)}$ and $\boldsymbol{q}^{(2)}$ can also be expressed by (3.11) but with the matrices $\boldsymbol{G}_1$ and $\boldsymbol{G}_2$ being given by

$$\begin{aligned}\boldsymbol{G}_1 &= -(\overline{\hat{\boldsymbol{A}}}^{(1)})^{-1}(\overline{\hat{\boldsymbol{M}}}^{(1)} + \hat{\boldsymbol{M}}^{(2)})^{-1}(\hat{\boldsymbol{M}}^{(1)} - \hat{\boldsymbol{M}}^{(2)})\hat{\boldsymbol{A}}^{(1)} \\ \boldsymbol{G}_2 &= (\hat{\boldsymbol{A}}^{(2)})^{-1}(\overline{\hat{\boldsymbol{M}}}^{(1)} + \hat{\boldsymbol{M}}^{(2)})^{-1}(\hat{\boldsymbol{M}}^{(1)} + \overline{\hat{\boldsymbol{M}}}^{(1)})\hat{\boldsymbol{A}}^{(1)}\end{aligned} \tag{3.14}$$

where $\hat{\boldsymbol{M}}^{(\alpha)}$ are the modified impedance tensors defined as

$$\hat{\boldsymbol{M}}^{(\alpha)} = -i\hat{\boldsymbol{B}}^{(\alpha)}(\hat{\boldsymbol{A}}^{(\alpha)})^{-1} \qquad (\alpha = 1, 2) \tag{3.15}$$

with the modified Stroh matrices $\hat{\boldsymbol{A}}^{(\alpha)}$ and $\hat{\boldsymbol{B}}^{(\alpha)}$ for the interface Model 2 being defined as

$$\hat{\boldsymbol{A}}^{(\alpha)} = \boldsymbol{A}^{(\alpha)} \qquad (\alpha = 1,2)$$

$$\hat{\boldsymbol{B}}^{(1)} = \begin{pmatrix} B_{11}^{(1)} & B_{12}^{(1)} & B_{13}^{(1)} & B_{14}^{(1)} \\ B_{21}^{(1)} & B_{22}^{(1)} & B_{23}^{(1)} & B_{24}^{(1)} \\ B_{31}^{(1)} & B_{32}^{(1)} & B_{33}^{(1)} & B_{34}^{(1)} \\ A_{41}^{(1)} & A_{42}^{(1)} & A_{43}^{(1)} & A_{44}^{(1)} \end{pmatrix}; \ \hat{\boldsymbol{B}}^{(2)} = \begin{pmatrix} B_{11}^{(2)} & B_{12}^{(2)} & B_{13}^{(2)} & B_{14}^{(2)} \\ B_{21}^{(2)} & B_{22}^{(2)} & B_{23}^{(2)} & B_{24}^{(2)} \\ B_{31}^{(2)} & B_{32}^{(2)} & B_{33}^{(2)} & B_{34}^{(2)} \\ -A_{41}^{(2)} & -A_{42}^{(2)} & -A_{43}^{(2)} & -A_{44}^{(2)} \end{pmatrix} \tag{3.16}$$

Following the same approach, the solution for the complex vectors $\overline{\boldsymbol{q}}^{(1)}$ and $\boldsymbol{q}^{(2)}$ for other four interface models can also be expressed by (3.14) with the matrices $\boldsymbol{G}_1$ and $\boldsymbol{G}_2$ being related to the modified Stroh matrices defined by (3.15). What we need to do is to find the modified Stroh matrices $\hat{\boldsymbol{A}}^{(\alpha)}$ and $\hat{\boldsymbol{B}}^{(\alpha)}$ for these models, which are given below.

Model 3:

$$\hat{\boldsymbol{A}}^{(1)} = \begin{pmatrix} A_{11}^{(1)} & A_{12}^{(1)} & A_{13}^{(1)} & A_{14}^{(1)} \\ A_{21}^{(1)} & A_{22}^{(1)} & A_{23}^{(1)} & A_{24}^{(1)} \\ A_{31}^{(1)} & A_{32}^{(1)} & A_{33}^{(1)} & A_{34}^{(1)} \\ B_{41}^{(1)} & B_{42}^{(1)} & B_{43}^{(1)} & B_{44}^{(1)} \end{pmatrix}; \ \hat{\boldsymbol{A}}^{(2)} = \begin{pmatrix} A_{11}^{(2)} & A_{12}^{(2)} & A_{13}^{(2)} & A_{14}^{(2)} \\ A_{21}^{(2)} & A_{22}^{(2)} & A_{23}^{(2)} & A_{24}^{(2)} \\ A_{31}^{(2)} & A_{32}^{(2)} & A_{33}^{(2)} & A_{34}^{(2)} \\ -B_{41}^{(2)} & -B_{42}^{(2)} & -B_{43}^{(2)} & -B_{44}^{(2)} \end{pmatrix} \tag{3.17}$$

$$\hat{\boldsymbol{B}}^{(\alpha)} = \boldsymbol{B}^{(\alpha)} \ (\alpha = 1,2)$$

Model 4:

$$\hat{\boldsymbol{A}}^{(1)} = \begin{pmatrix} B_{11}^{(1)} & B_{12}^{(1)} & B_{13}^{(1)} & B_{14}^{(1)} \\ B_{21}^{(1)} & B_{22}^{(1)} & B_{23}^{(1)} & B_{24}^{(1)} \\ A_{31}^{(1)} & A_{32}^{(1)} & A_{33}^{(1)} & A_{34}^{(1)} \\ A_{41}^{(1)} & A_{42}^{(1)} & A_{43}^{(1)} & A_{44}^{(1)} \end{pmatrix}; \ \hat{\boldsymbol{A}}^{(2)} = \begin{pmatrix} -B_{11}^{(2)} & -B_{12}^{(2)} & -B_{13}^{(2)} & -B_{14}^{(2)} \\ -B_{21}^{(2)} & -B_{22}^{(2)} & -B_{23}^{(2)} & -B_{24}^{(2)} \\ A_{31}^{(2)} & A_{32}^{(2)} & A_{33}^{(2)} & A_{34}^{(2)} \\ A_{41}^{(2)} & A_{42}^{(2)} & A_{43}^{(2)} & A_{44}^{(2)} \end{pmatrix} \tag{3.18}$$

$$\hat{\boldsymbol{B}}^{(\alpha)} = \boldsymbol{B}^{(\alpha)} \ (\alpha = 1,2)$$

Model 5:

$$\hat{\boldsymbol{A}}^{(1)}=\begin{pmatrix} B_{11}^{(1)} & B_{12}^{(1)} & B_{13}^{(1)} & B_{14}^{(1)} \\ B_{21}^{(1)} & B_{22}^{(1)} & B_{23}^{(1)} & B_{24}^{(1)} \\ A_{31}^{(1)} & A_{32}^{(1)} & A_{33}^{(1)} & A_{34}^{(1)} \\ A_{41}^{(1)} & A_{42}^{(1)} & A_{43}^{(1)} & A_{44}^{(1)} \end{pmatrix};\ \hat{\boldsymbol{A}}^{(2)}=\begin{pmatrix} -B_{11}^{(2)} & -B_{12}^{(2)} & -B_{13}^{(2)} & -B_{14}^{(2)} \\ -B_{21}^{(2)} & -B_{22}^{(2)} & -B_{23}^{(2)} & -B_{24}^{(2)} \\ A_{31}^{(2)} & A_{32}^{(2)} & A_{33}^{(2)} & A_{34}^{(2)} \\ -A_{41}^{(2)} & -A_{42}^{(2)} & -A_{43}^{(2)} & -A_{44}^{(2)} \end{pmatrix} \tag{3.19}$$

$$\hat{\boldsymbol{B}}^{(1)}=\begin{pmatrix} B_{11}^{(1)} & B_{12}^{(1)} & B_{13}^{(1)} & B_{14}^{(1)} \\ B_{21}^{(1)} & B_{22}^{(1)} & B_{23}^{(1)} & B_{24}^{(1)} \\ B_{31}^{(1)} & B_{32}^{(1)} & B_{33}^{(1)} & B_{34}^{(1)} \\ A_{41}^{(1)} & A_{42}^{(1)} & A_{43}^{(1)} & A_{44}^{(1)} \end{pmatrix};\ \hat{\boldsymbol{B}}^{(2)}=\begin{pmatrix} B_{11}^{(2)} & B_{12}^{(2)} & B_{13}^{(2)} & B_{14}^{(2)} \\ B_{21}^{(2)} & B_{22}^{(2)} & B_{23}^{(2)} & B_{24}^{(2)} \\ B_{31}^{(2)} & B_{32}^{(2)} & B_{33}^{(2)} & B_{34}^{(2)} \\ A_{41}^{(2)} & A_{42}^{(2)} & A_{43}^{(2)} & A_{44}^{(2)} \end{pmatrix}$$

Model 6:

$$\hat{\boldsymbol{A}}^{(1)}=\begin{pmatrix} B_{11}^{(1)} & B_{12}^{(1)} & B_{13}^{(1)} & B_{14}^{(1)} \\ B_{21}^{(1)} & B_{22}^{(1)} & B_{23}^{(1)} & B_{24}^{(1)} \\ A_{31}^{(1)} & A_{32}^{(1)} & A_{33}^{(1)} & A_{34}^{(1)} \\ B_{41}^{(1)} & B_{42}^{(1)} & B_{43}^{(1)} & B_{44}^{(1)} \end{pmatrix};\ \hat{\boldsymbol{A}}^{(2)}=\begin{pmatrix} -B_{11}^{(2)} & -B_{12}^{(2)} & -B_{13}^{(2)} & -B_{14}^{(2)} \\ -B_{21}^{(2)} & -B_{22}^{(2)} & -B_{23}^{(2)} & -B_{24}^{(2)} \\ A_{31}^{(2)} & A_{32}^{(2)} & A_{33}^{(2)} & A_{34}^{(2)} \\ -B_{41}^{(2)} & -B_{42}^{(2)} & -B_{43}^{(2)} & -B_{44}^{(2)} \end{pmatrix} \tag{3.20}$$

$$\hat{\boldsymbol{B}}^{(\alpha)}=\boldsymbol{B}^{(\alpha)}\ (\alpha=1,2)$$

In summary, equations (3.3)-(3.5) are the bimaterial Green's functions for the extended displacements and stresses in the Fourier transformed domain. For the six different interface models, the complex vectors $\overline{\boldsymbol{q}}^{(1)}$ and $\boldsymbol{q}^{(2)}$ in (3.3)-(3.5) have been derived in a unified form by introducing the corresponding modified bimaterial Stroh matrices. With the exception of the bimaterial Green's functions for the perfect-bond interface Model 1, the bimaterial Green's functions for other five interface models are new and are obtained *for the first time*. Similar to the perfect-bond bimaterial Green's functions (Pan and Yuan, 2000), there are several important features pertaining to these Green's functions. While a detailed discussion can be found in Pan and Yuan (2000) for the perfect-bond interface case, we re-state only one of the features closely related to the this work and present three new observations associated with the more general interface conditions:

(1) The first term in (3.3) and (3.4) is the Fourier-domain Green's function for the anisotropic and piezoelectric full-space. Since the corresponding physical-domain solution has been developed by Akamatsu and Tanuma (1997) and Pan and Tonon (2000) in an explicit form, the Fourier inverse transform needs to be carried out only for the second term of the solutions, which is similar to the complementary part of the Mindlin solution (1936).

(2) The modified Stroh matrices are introduced *only* for the purpose of determining the complex vectors $\overline{\boldsymbol{q}}^{(1)}$ and $\boldsymbol{q}^{(2)}$. The matrices $\boldsymbol{A}$, $\boldsymbol{B}$, and $\boldsymbol{C}$ in (3.3)-(3.5) and later in the final expressions for the physical-domain Green's functions (i.e., equations (5.1), (5.2), and (5.5)) are the original and should not be modified.

(3) The methodology is not restricted to the six interface models presented in this paper. The complex vectors $\overline{\boldsymbol{q}}^{(1)}$ and $\boldsymbol{q}^{(2)}$ in (3.3)-(3.5) for other interface models can be derived similarly by introducing the corresponding modified Stroh matrices, provided that the extended displacement and traction components are uncoupled in the interface conditions.

(4) Under the assumption of 2D deformation, the corresponding anisotropic and piezoelectric bimaterial Green's functions in the physical domain with the six interface models can be derived in exact-closed form using directly the 3D bimaterial Stroh matrices at the fixed polar angle θ=0. This is developed in Appendix A of this paper.

4. Bimaterial Green's Functions in the Physical Domain

Having obtained the bimaterial Green's functions in the transformed domain, we now apply the inverse Fourier transform to equations (3.3)-(3.5). To handle the double infinite integrals, the polar coordinate transform (3.2) is applied so that the infinite integral with respect to the radial variable can be carried out exactly. Thus, the final bimaterial Green's functions in the physical domain can be expressed in terms of a regular line-integral over [0, 2π], which can be further reduced to [0, π] using certain properties of the Stroh eigenvalues and Stroh matrices (Pan, 2002a). The procedure is very similar to the interface Model 1 solved previously by Pan and Yuan (2000), and one needs only to replace the matrices $\boldsymbol{G}_1$ and $\boldsymbol{G}_2$ with those corresponding to the given interface conditions. Therefore, we only list the final results while a similar and detailed derivation can be found in Pan and Yuan (2000) for the piezoelectric bimaterials with perfect-bond interface Model 1. We further emphasize that the modified bimaterial Stroh matrices are used only in the expressions for the matrices $\boldsymbol{G}_1$ and $\boldsymbol{G}_2$.

Assuming that $z \neq 0$ or $d \neq 0$, the 4×4 Green's function tensor, with its first index for the extended displacement component and the second for the extended point-force direction, is found to be

$$\boldsymbol{U}^{(1)}(\boldsymbol{x};\boldsymbol{d}) = \boldsymbol{U}^{\infty}(\boldsymbol{x};\boldsymbol{d}) + \frac{1}{2\pi^2}\left[\int_0^{\pi} \overline{\boldsymbol{A}}^{(1)}\boldsymbol{G}_u^{(1)}(\boldsymbol{A}^{(1)})^T d\theta\right] \tag{4.1}$$

$$(\boldsymbol{G}_u^{(1)})_{IJ} = \frac{(\boldsymbol{G}_1)_{IJ}}{-\overline{p}_I^{(1)} z + p_J^{(1)} d - [(x_1 - d_1)\cos\theta + (x_2 - d_2)\sin\theta]} \tag{4.2}$$

In equation (4.1), $\boldsymbol{U}^{\infty}(\boldsymbol{x};\boldsymbol{d})$ denotes the Green's function tensor for the extended displacements in the full-space with material 1 (Pan and Tonon, 2000), and in equation (4.2), the indices I and J take the range from 1 to 4. Similarly, the bimaterial Green's functions for the extended stresses (traction and in-plane stress) can be derived as:

$$\begin{aligned} \boldsymbol{T}^{(1)}(\boldsymbol{x};\boldsymbol{d}) &= \boldsymbol{T}^{\infty}(\boldsymbol{x};\boldsymbol{d}) + \frac{1}{2\pi^2}\left[\int_0^{\pi} \overline{\boldsymbol{B}}^{(1)}\boldsymbol{G}_t^{(1)}(\boldsymbol{A}^{(1)})^T d\theta\right] \\ \boldsymbol{S}^{(1)}(\boldsymbol{x};\boldsymbol{d}) &= \boldsymbol{S}^{\infty}(\boldsymbol{x};\boldsymbol{d}) + \frac{1}{2\pi^2}\left[\int_0^{\pi} \overline{\boldsymbol{C}}^{(1)}\boldsymbol{G}_t^{(1)}(\boldsymbol{A}^{(1)})^T d\theta\right] \end{aligned} \tag{4.3}$$

$$\boldsymbol{U}^{(2)}(\boldsymbol{x};\boldsymbol{d}) = -\frac{1}{2\pi^2}\left[\int_0^{\pi} \boldsymbol{A}^{(2)}\boldsymbol{G}_u^{(2)}(\boldsymbol{A}^{(1)})^T d\theta\right]$$
$$\boldsymbol{T}^{(2)}(\boldsymbol{x};\boldsymbol{d}) = -\frac{1}{2\pi^2}\left[\int_0^{\pi} \boldsymbol{B}^{(2)}\boldsymbol{G}_t^{(2)}(\boldsymbol{A}^{(1)})^T d\theta\right] \tag{4.4}$$
$$\boldsymbol{S}^{(2)}(\boldsymbol{x};\boldsymbol{d}) = -\frac{1}{2\pi^2}\left[\int_0^{\pi} \boldsymbol{C}^{(2)}\boldsymbol{G}_t^{(2)}(\boldsymbol{A}^{(1)})^T d\theta\right]$$

In equation (4.3), $\boldsymbol{T}^{\infty}(\boldsymbol{x};\boldsymbol{d})$ and $\boldsymbol{S}^{\infty}(\boldsymbol{x};\boldsymbol{d})$ are the Green's functions for the extended stresses in the full-space with material 1 (Pan and Tonon, 2000), and

$$(\boldsymbol{G}_t^{(1)})_{IJ} = \frac{(\boldsymbol{G}_1)_{IJ}}{\{-\overline{p}_{\mathrm{I}}^{(1)} z + p_{\mathrm{J}}^{(1)} d - [(x_1 - d_1)\cos\theta + (x_2 - d_2)\sin\theta]\}^2} \tag{4.5}$$

$$(\boldsymbol{G}_u^{(2)})_{IJ} = \frac{(\boldsymbol{G}_2)_{IJ}}{-\,p_{\mathrm{I}}^{(2)} z + p_{\mathrm{J}}^{(1)} d - [(x_1 - d_1)\cos\theta + (x_2 - d_2)\sin\theta)]} \tag{4.6}$$

$$(\boldsymbol{G}_t^{(2)})_{IJ} = \frac{(\boldsymbol{G}_2)_{IJ}}{\{-p_{\mathrm{I}}^{(2)} z + p_{\mathrm{J}}^{(1)} d - [(x_1 - d_1)\cos\theta + (x_2 - d_2)\sin\theta]\}^2} \tag{4.7}$$

Therefore, in material 1, the bimaterial Green's function is expressed as a sum of the explicit full-space Green's function and a complementary part in terms of a line integral over [0, π]; In material 2, the bimaterial Green's function is expressed in terms of a line integral over [0, π]. Concerning the complicated nature of the problem and the final concise expression for the bimaterial Green's function, it is concluded that the extended Stroh formalism is truly mathematically elegant and numerically powerful (Ting, 1996), especially when used jointly with the modified bimaterial Stroh matrices introduced in this paper. Furthermore, with regard to these physical-domain bimaterial Green's functions (i.e., equations (4.1), (4.3), and (4.4)), the following important observations can be made, with some of them being similar to those made in Pan and Yuan (2000):

(1) For the complementary part of the solution in material 1 and the solution in material 2, the dependence of the solutions on the field point $\boldsymbol{x}$ and source point $\boldsymbol{d}$ appears only through matrices $\boldsymbol{G}_u^{(1)}$, $\boldsymbol{G}_t^{(1)}$, $\boldsymbol{G}_u^{(2)}$, and $\boldsymbol{G}_t^{(2)}$ defined in (4.2) and (4.5)-(4.7).

(2) The integrals in (4.1), (4.3), and (4.4) are regular if $z \neq 0$ or $d \neq 0$, and thus can be easily carried out by a standard numerical integral method such as the Gauss quadrature.

(3) If $z \neq 0$ and $d = 0$, the bimaterial Green's function is still mathematically regular although some of its components may not have a direct and apparent physical meaning (see, Dundurs and Hetenyi, 1965, for the purely elastic counterpart).

(4) When the field and source points are both on the interface (i.e., $z = d = 0$), the bimaterial Green's function is then reduced to the interfacial Green's function. For this special case, the line integral involved in the Green's function expression becomes singular and the resulting finite-part integral needs to be handled with special cares (Pan and Yang, 2003).

5. Effects of Interface Conditions

Effect of different interface conditions on the mechanical and electrical fields has never been studied in the literature when the mechanical and piezoelectric coupling is involved. This effect, however, is very important in the piezoelectric composite design and in the modeling of advanced electronic quantum devices. In the following, we offer a systematic discussion on this issue based on the solution derived above. It is seen that the effects of different interface conditions can be studied in a unified and concise form.

Similar to the generalized Mindlin problem in an anisotropic and piezoelectric half space with general boundary conditions (Pan, 2002a), the infinite-space Green's function is found to have no influence on the correction to, or difference of, the mechanical and electronic quantities arising from different interface conditions. It is the complementary part of the bimaterial solution that contributes to the correction, which is in turn controlled by the matrix $\boldsymbol{G}_1$ or $\boldsymbol{G}_2$.

In the study presented below, we restrict ourselves to the case where the source point $\boldsymbol{d}$ is within material 1 ($d > 0$) but the field point $\boldsymbol{x}$ can be anywhere in the bimaterials. Furthermore, the correction is relative to the bimaterial Green's function corresponding to the perfect-bond interface Model 1. We also mention that results for the derivatives of the extended displacements and stresses will not be given but can be obtained trivially.

For the field point in material 1 (i.e., $z > 0$), we found that

$$\boldsymbol{U}^{(1)}(\boldsymbol{x};\boldsymbol{d})\,|_M - \boldsymbol{U}^{(1)}(\boldsymbol{x};\boldsymbol{d})\,|_1 = \frac{1}{2\pi^2}\left[\int_0^{\pi} \overline{\boldsymbol{A}}^{(1)} \Delta \boldsymbol{G}_u^{(1)} (\boldsymbol{A}^{(1)})^T d\theta\right] \tag{5.1}$$

$$\begin{aligned} \boldsymbol{T}^{(1)}(\boldsymbol{x};\boldsymbol{d})\,|_M - \boldsymbol{T}^{(1)}(\boldsymbol{x};\boldsymbol{d})\,|_1 &= \frac{1}{2\pi^2}\left[\int_0^{\pi} \overline{\boldsymbol{B}}^{(1)} \Delta \boldsymbol{G}_t^{(1)} (\boldsymbol{A}^{(1)})^T d\theta\right] \\ \boldsymbol{S}^{(1)}(\boldsymbol{x};\boldsymbol{d})|_M - \boldsymbol{S}^{(1)}(\boldsymbol{x};\boldsymbol{d})|_1 &= \frac{1}{2\pi^2}\left[\int_0^{\pi} \overline{\boldsymbol{C}}^{(1)} \Delta \boldsymbol{G}_t^{(1)} (\boldsymbol{A}^{(1)})^T d\theta\right] \end{aligned} \tag{5.2}$$

where

$$(\Delta \boldsymbol{G}_u^{(1)})_{IJ} = \frac{(\boldsymbol{G}_1\,|_K - \boldsymbol{G}_1\,|_1)_{IJ}}{-\overline{p}_{\mathrm{I}}^{(1)} z + p_{\mathrm{J}}^{(1)} d - [(x_1 - d_1)\cos\theta + (x_2 - d_2)\sin\theta]} \tag{5.3}$$

$$(\Delta \boldsymbol{G}_t^{(1)})_{IJ} = \frac{(\boldsymbol{G}_1\,|_K - \boldsymbol{G}_1\,|_1)_{IJ}}{\{-\overline{p}_{\mathrm{I}}^{(1)} z + p_{\mathrm{J}}^{(1)} d - [(x_1 - d_1)\cos\theta + (x_2 - d_2)\sin\theta]\}^2} \tag{5.4}$$

In equations (5.1)-(5.4), the extended displacement and stress fields with a vertical line followed by the subscript 1 are the bimaterial Green's functions corresponding to the interface Model 1, and those followed by the subscript M (=2, 3, 4, 5, and 6) correspond to the other five interface models.

Similarly, for the field point in material 2 (i.e., $z < 0$), the corrections are

$$\begin{aligned}
\boldsymbol{U}^{(2)}(\boldsymbol{x};\boldsymbol{d})|_M - \boldsymbol{U}^{(2)}(\boldsymbol{x};\boldsymbol{d})|_1 &= -\frac{1}{2\pi^2}\left[\int_0^{\pi} \boldsymbol{A}^{(2)}\Delta\boldsymbol{G}_u^{(2)}(\boldsymbol{A}^{(1)})^T d\theta\right] \\
\boldsymbol{T}^{(2)}(\boldsymbol{x};\boldsymbol{d})|_M - \boldsymbol{T}^{(2)}(\boldsymbol{x};\boldsymbol{d})|_1 &= -\frac{1}{2\pi^2}\left[\int_0^{\pi} \boldsymbol{B}^{(2)}\Delta\boldsymbol{G}_t^{(2)}(\boldsymbol{A}^{(1)})^T d\theta\right] \\
\boldsymbol{S}^{(2)}(\boldsymbol{x};\boldsymbol{d})|_M - \boldsymbol{S}^{(2)}(\boldsymbol{x};\boldsymbol{d})|_1 &= -\frac{1}{2\pi^2}\left[\int_0^{\pi} \boldsymbol{C}^{(2)}\Delta\boldsymbol{G}_t^{(2)}(\boldsymbol{A}^{(1)})^T d\theta\right]
\end{aligned} \tag{5.5}$$

where

$$(\Delta\boldsymbol{G}_u^{(2)})_{IJ} = \frac{(\boldsymbol{G}_2|_K - \boldsymbol{G}_2|_1)_{IJ}}{-p_{\mathrm{I}}^{(2)}z + p_{\mathrm{J}}^{(1)}d - [(x_1-d_1)\cos\theta + (x_2-d_2)\sin\theta)]} \tag{5.6}$$

$$(\Delta\boldsymbol{G}_t^{(2)})_{IJ} = \frac{(\boldsymbol{G}_2|_K - \boldsymbol{G}_2|_1)_{IJ}}{\{-p_{\mathrm{I}}^{(2)}z + p_{\mathrm{J}}^{(1)}d - [(x_1-d_1)\cos\theta + (x_2-d_2)\sin\theta]\}^2} \tag{5.7}$$

These results (i.e., equations (5.1)-(5.7)) are believed to be new, and should be particularly useful when studying the effect of different interface models on the mechanical and electrical fields. Furthermore, the exact-closed form Green's functions derived in Appendix A for the corresponding 2D bimaterial case with the six different interface models enable one to carry out various parametric studies on the effect of different interface conditions using the expression similar to (5.1), (5.2), and (5.5). Numerical examples in the next section for the 3D bimaterial Green's functions show several new features that could be of special interest.

6. Numerical Examples

Having derived the bimaterial Green's function and discussed the effect of different interface conditions on the mechanical and electrical quantities, we now illustrate some of the Green's components by numerical examples. Two typical piezoelectric materials (Pan, 2002a) are selected for the bimaterial full-space: One is a left-hand quartz in a rotated coordinate system (Tiersten, 1969) with elastic constants, piezoelectric coefficients, and dielectric constants being, respectively,

$$[C] = \begin{bmatrix} .8674 & -.0825 & .2715 & -.0366 & 0 & 0 \\ -.0825 & 1.2977 & -.0742 & .057 & 0 & 0 \\ .2715 & -.0742 & 1.0283 & .0992 & 0 & 0 \\ -.0366 & .057 & .0992 & .3861 & 0 & 0 \\ 0 & 0 & 0 & 0 & .6881 & .0253 \\ 0 & 0 & 0 & 0 & .0253 & .2901 \end{bmatrix} (10^{11}\, N/m^2) \tag{6.1}$$

$$[e] = \begin{bmatrix} .171 & -.152 & -.0187 & .067 & 0 & 0 \\ 0 & 0 & 0 & 0 & .108 & -.095 \\ 0 & 0 & 0 & 0 & -.0761 & .067 \end{bmatrix} (C/m^2) \tag{6.2}$$

$$[\varepsilon]=\begin{bmatrix} .3921 & 0 & 0 \\ 0 & .3982 & .0086 \\ 0 & .0086 & .4042 \end{bmatrix}(10^{-10}C/Vm) \tag{6.3}$$

Another one is the poled lead-zirconate-titanate (PZT-4) ceramic (Dunn and Taya, 1993) with elastic constants, piezoelectric coefficients, and dielectric constants being, respectively,

$$[C]=\begin{bmatrix} 1.39 & .778 & .743 & 0 & 0 & 0 \\ .778 & 1.39 & .743 & 0 & 0 & 0 \\ .743 & .743 & 1.15 & 0 & 0 & 0 \\ 0 & 0 & 0 & .256 & 0 & 0 \\ 0 & 0 & 0 & 0 & .256 & 0 \\ 0 & 0 & 0 & 0 & 0 & .306 \end{bmatrix}(10^{11}N/m^2) \tag{6.4}$$

$$[e]=\begin{bmatrix} 0 & 0 & 0 & 0 & 12.7 & 0 \\ 0 & 0 & 0 & 12.7 & 0 & 0 \\ -5.2 & -5.2 & 15.1 & 0 & 0 & 0 \end{bmatrix}(C/m^2) \tag{6.5}$$

$$[\varepsilon]=\begin{bmatrix} .64605 & 0 & 0 \\ 0 & .64605 & 0 \\ 0 & 0 & .561975 \end{bmatrix}(10^{-8}C/Vm) \tag{6.6}$$

It is noted that while the quartz is a weakly coupled piezoelectric material, the ceramic is a strongly coupled one, with the degree of the electromechanical coupling, defined as $g=e_{\max}/\sqrt{(\varepsilon_{\max}C_{\max})}$, being equal to 0.07 and 0.5, respectively.

Numerical results are presented for the elastic stress and electrical displacement, caused by a point force of 1N/m^3 or a negative point electrical charge of 1C/m^3. While the source is fixed at $\boldsymbol{d}$=(0,0,1m) in material 1 (i.e., the upper half-space with z>0), the field point varies along a vertical line as $\boldsymbol{x}$=(1m,1m,z), $z\in$[-3m,3m]. Two bimaterial systems are considered: For system 1, materials 1 and 2 are, respectively, ceramic and quartz, denoted by ceramic/quartz; whilst for system 2, materials 1 and 2 are, respectively, quartz and ceramic, denoted by quartz/ceramic.

In each figure, six curves are plotted, with M1 to M6 corresponding to the interface Models 1 to 6, respectively, and with the results for the interface Model 1 being the same as those reported by Pan and Yuan (2000). By presenting the results for all the interface models, the corrections to the field quantities due to different interface models, discussed in the previous section, can be observed directly from these figures. Furthermore, according to the field and source types, the numerical results are grouped into four cases and are discussed below:

1). Electrical response due to a mechanical point source:

Figures 2a and 2b show, respectively, the variation of the electrical displacements D_x and D_z along the vertical line $\boldsymbol{x}$=(1m,1m,z) in the ceramic/quartz bimaterials due to a point force in the z-direction (i.e. Fz). The corresponding D_x and D_z in the quartz/ceramic bimaterials are plotted in Figures 2c and 2d. It is observed from these figures that when a

mechanical point source is applied, different interface models can produce significantly different electrical responses in the strongly electromechanically coupled ceramic half-space. However, a mechanical point source causes negligible electrical displacements in the weakly coupling quartz half-space for all six different interface models. Furthermore, the effect of different interface models on the electrical displacement in the ceramic half-space due to a mechanical point source in the same half-space is very strong, with different interface models predicting quite different amplitudes for the electrical displacement. A final feature, as shown in Figures 2c and 2d and may be useful when designing piezoelectric composites, is that even when a mechanical force is applied in the weakly coupled quartz domain, a substantial electrical displacement can still be produced in the adjacent ceramic domain, with different amplitudes and even different shapes.

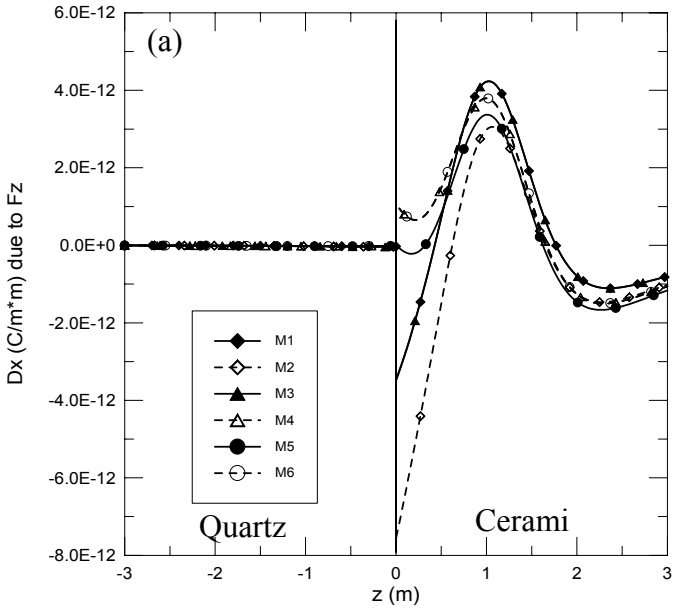

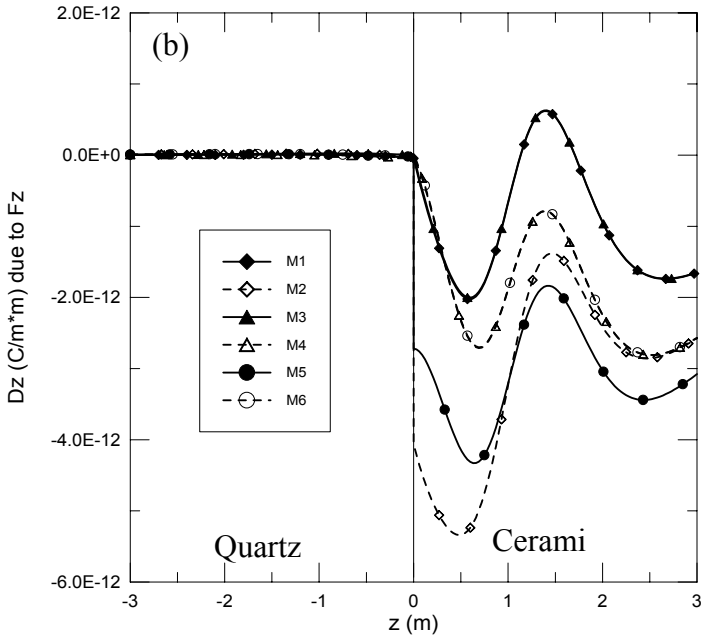
(b)
2.0E-12
0.0E+0
-2.0E-12
-4.0E-12
-6.0E-12
Dz (C/m*m) due to Fz
M1
M2
M3
M4
M5
M6
Quartz
Cerami
-3
-2
-1
0
1
2
3
z (m)

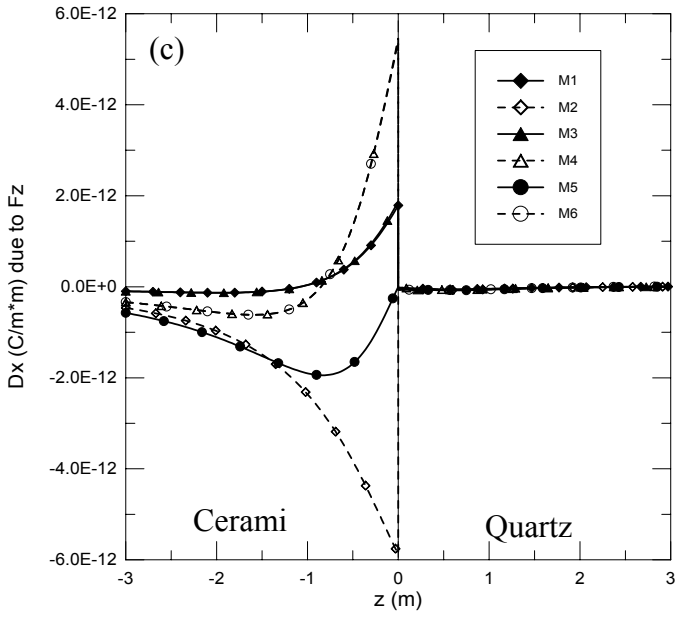
(c)
6.0E-12
4.0E-12
2.0E-12
0.0E+0
-2.0E-12
-4.0E-12
-6.0E-12
Dx (C/m*m) due to Fz
M1
M2
M3
M4
M5
M6
Cerami
Quartz
-3
-2
-1
0
1
2
3
z (m)

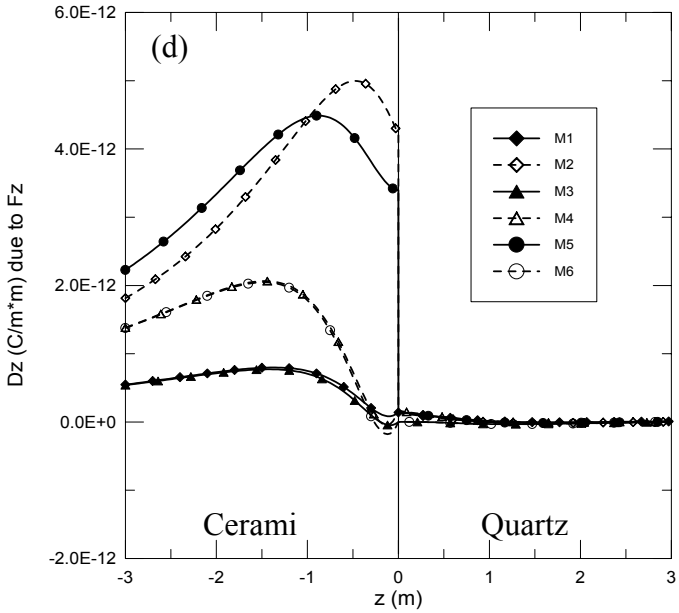

Figure 2. Variations of electrical displacements D_x and D_z along vertical line $\boldsymbol{x}$=(1m,1m,z) in the ceramic/quartz bimaterials (a & b) and quartz/ceramic bimaterials (c & d) due to a point force of 1N/m^3 applied at $\boldsymbol{d}$=(0,0,1m) in the z-direction. Curves M1 to M6 correspond to the interface Models 1 to 6, respectively.

2). Mechanical response due to an electrical point source:

While Figures 3a and 3b show, respectively, the variation of the elastic stress components σ_{xx} and σ_{zz} along the vertical line $\boldsymbol{x}$=(1m,1m,z) in the ceramic/quartz bimaterials due to a negative point electrical charge (i.e., F4), Figures 3c and 3d show the corresponding variation of σ_{xx} and σ_{zz} in the quartz/ceramic bimaterials. Similar to the first case, different interface models can have a great influence on the stress distribution when a point electrical source is applied. In other words, it is possible to produce certain required stress responses when an electrical point source is applied to a piezoelectric bimaterial system if different interface models are incorporated into the design plan. Furthermore, two interesting features can be observed from Figures 3a and 3b: First, the interface Models 1 and 3 (mechanical perfect-bond), and Models 4 and 6 (mechanical smooth-bond) predict, respectively, nearly identical stresses (components σ_{xx} and σ_{zz}), implying that, in this situation, the normal stress field alone cannot differentiate the electrically open interface condition from the perfect-bond electrical interface condition (i.e., the electrical potential and the normal electrical displacement component are continuous across the interface). Second, when an electrical point source is applied in the strongly coupled ceramic half-space, the responses of the normal stress component σ_{zz} in both half-spaces are roughly divided into two groups (Figure 3b): One is related to the interface Models 2 and 5, and the other to the other four interface models. Since Models

2 and 5 have the same electrical interface condition, i.e., electrically closed interface, we conclude that the normal stress component σ_{zz} in both half spaces is mainly controlled by the electrically closed interface condition; Other two types of electrical interface conditions as well as the two mechanical interface conditions have only a weak effect on this stress component.

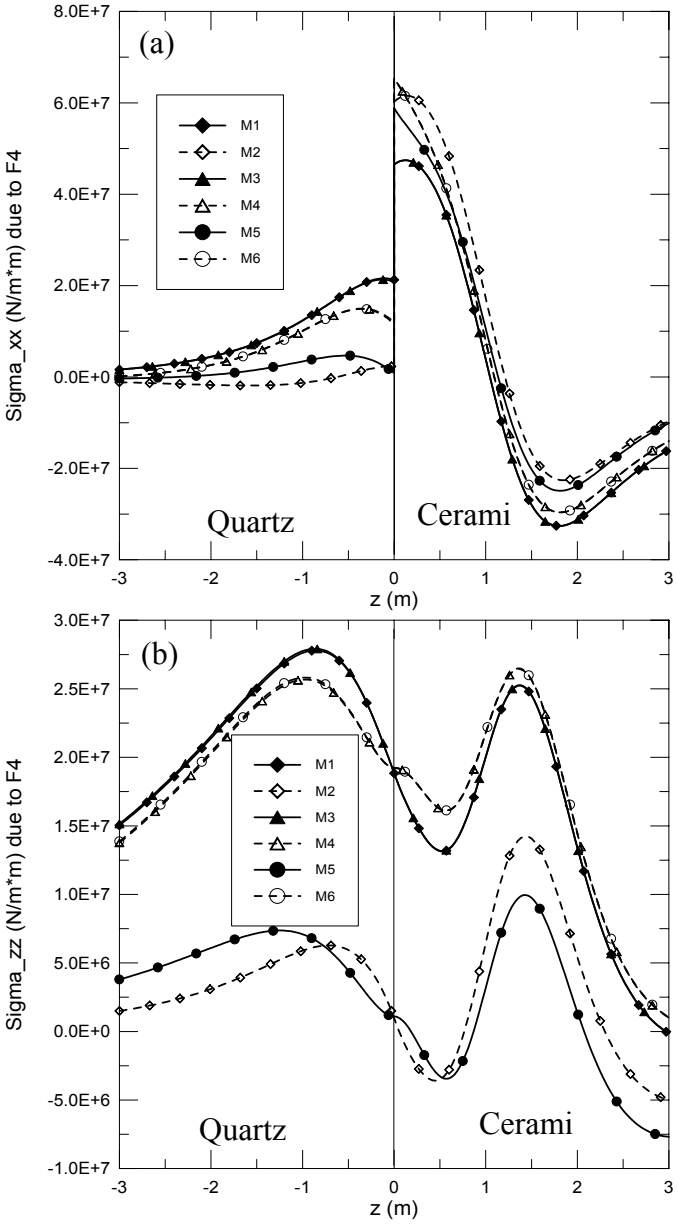

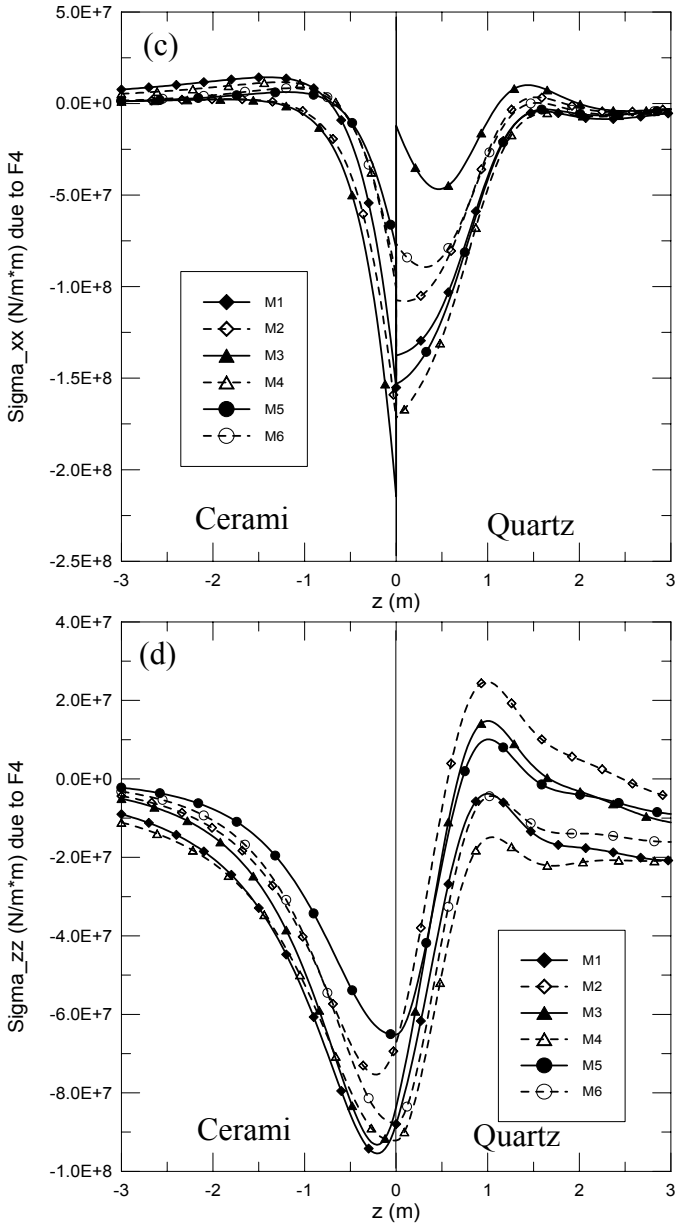

Figure 3. Variations of stress components σ_{xx} and σ_{zz} along vertical line $\boldsymbol{x}$ =(1m,1m,z) in the ceramic/quartz bimaterials (a & b) and quartz/ceramic bimaterials (c & d) due to a negative point electrical charge of 1C/m^3 applied at $\boldsymbol{d}$=(0,0,1m). Curves M1 to M6 correspond to the interface Models 1 to 6, respectively.

3). Electrical response due to an electrical point source:

Figures 4a and 4b show the variation of the electrical displacement components D_x and D_z, respectively, along the vertical line $\boldsymbol{x}$=(1m,1m,z) in the ceramic/quartz bimaterials due to a negative point electrical charge. The corresponding D_x and D_z in the quartz/ceramic bimaterials are plotted in Figures 4c and 4d. It is very interesting that for the ceramic/quartz bimaterials (i.e., Figures 4a and 4b), while the electrical displacements in the quartz half-space are negligible, those in the ceramic half space (i.e. in the source half space) clearly fall into two groups with one corresponding to Models 2 and 5, and the other to the remaining four interface models. That is, for this situation, the electrical response due to an electrical point source is very sensitive to the electrically closed interface condition; the electrical displacements due to other mechanical or electrical interface conditions all predict nearly identical results. If, however, the bimaterial system is quartz/ceramic, then the result becomes quite different (Figures 4a and 4b): In the ceramic half-space, i.e., the source-free half space, the distributions of the electrical displacements are different for different interface models; In the source-loaded half space (i.e., in the quartz half space), on the other hand, the responses are clearly separated into two groups: one corresponds to the interface Models 3 and 6, and the other to other four interface models. In other words, for this situation and in the weakly electromechanically coupled source-loaded half-space, the electrical displacement is very sensitive to the electrically open interface condition; Responses due to other interface conditions are very close to each other.

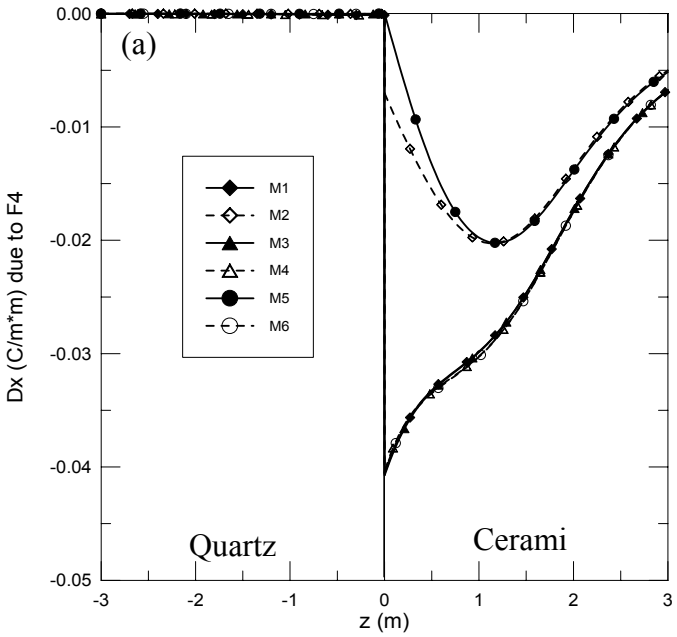

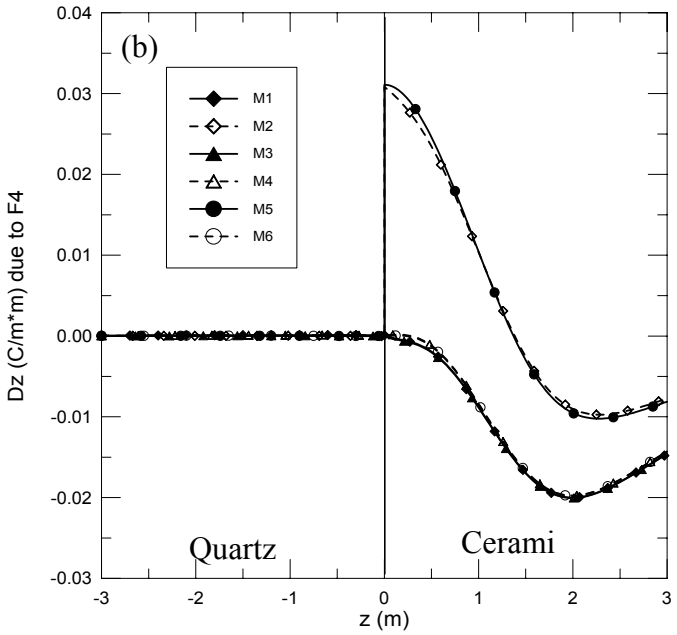
(b)
M1
M2
M3
M4
M5
M6
Dz (C/m*m) due to F4
z (m)
Quartz
Cerami
0.04
0.03
0.02
0.01
0.00
-0.01
-0.02
-0.03
-3
-2
-1
0
1
2
3

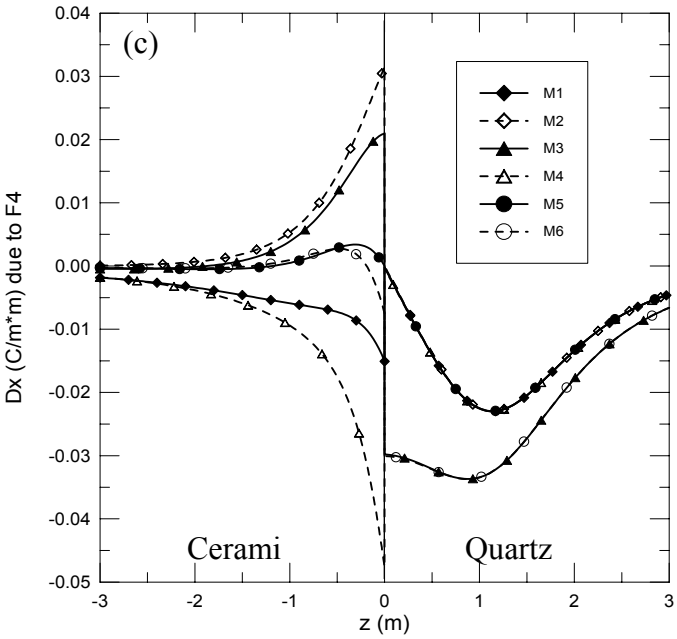
(c)
M1
M2
M3
M4
M5
M6
Dx (C/m*m) due to F4
z (m)
Cerami
Quartz
0.04
0.03
0.02
0.01
0.00
-0.01
-0.02
-0.03
-0.04
-0.05
-3
-2
-1
0
1
2
3

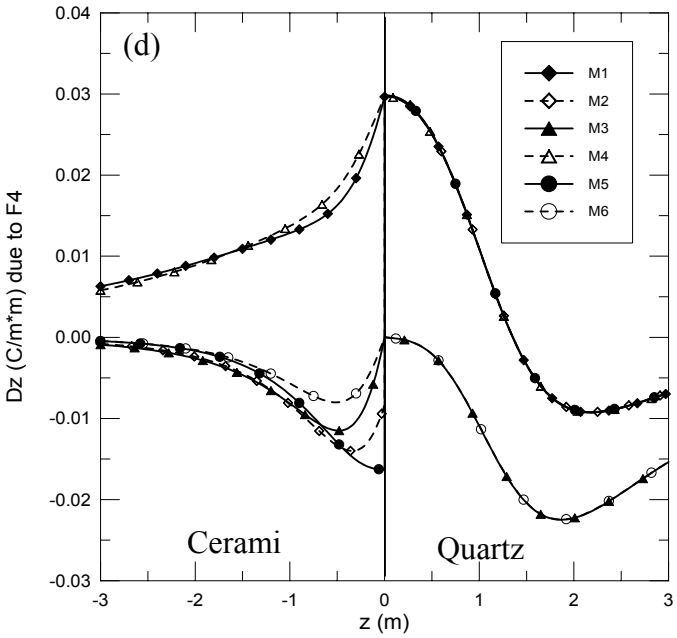

Figure 4. Variations of electrical displacement components D_x and D_z along vertical line $\boldsymbol{x}$=(1m,1m,z) in the ceramic/quartz bimaterials (a & b) and quartz/ceramic bimaterials (c & d) due to a negative point electrical charge of 1C/m^3 applied at $\boldsymbol{d}$=(0,0,1m). Curves M1 to M6 correspond to the interface Models 1 to 6, respectively.

4). Mechanical response due to a mechanical point source:

While the stress components σ_{xx} and σ_{zz} along the vertical line $\boldsymbol{x}$=(1m,1m,z) in the ceramic/quartz bimaterials due to a point force in the z-direction are plotted, respectively, in Figures 5a and 5b, the corresponding σ_{xx} and σ_{zz} in the quartz/ceramic bimaterials are depicted in Figures 5c and 5d. It is apparent that, the stresses are more or less divided into two groups that are mainly controlled by the mechanical perfect-bond and smooth-bond interface conditions. The electrical interface conditions have only a weakly influence on the stress distribution, with the stresses from interface Models 2 and 5 (with mechanical perfect-bond and smooth-bond respectively, but with electrically closed interface for both) being slightly distinct from these two groups (Figure 5a-5d). This means that in certain situations, the electrically closed interface condition may disturb the stress distributions due to a mechanical source.

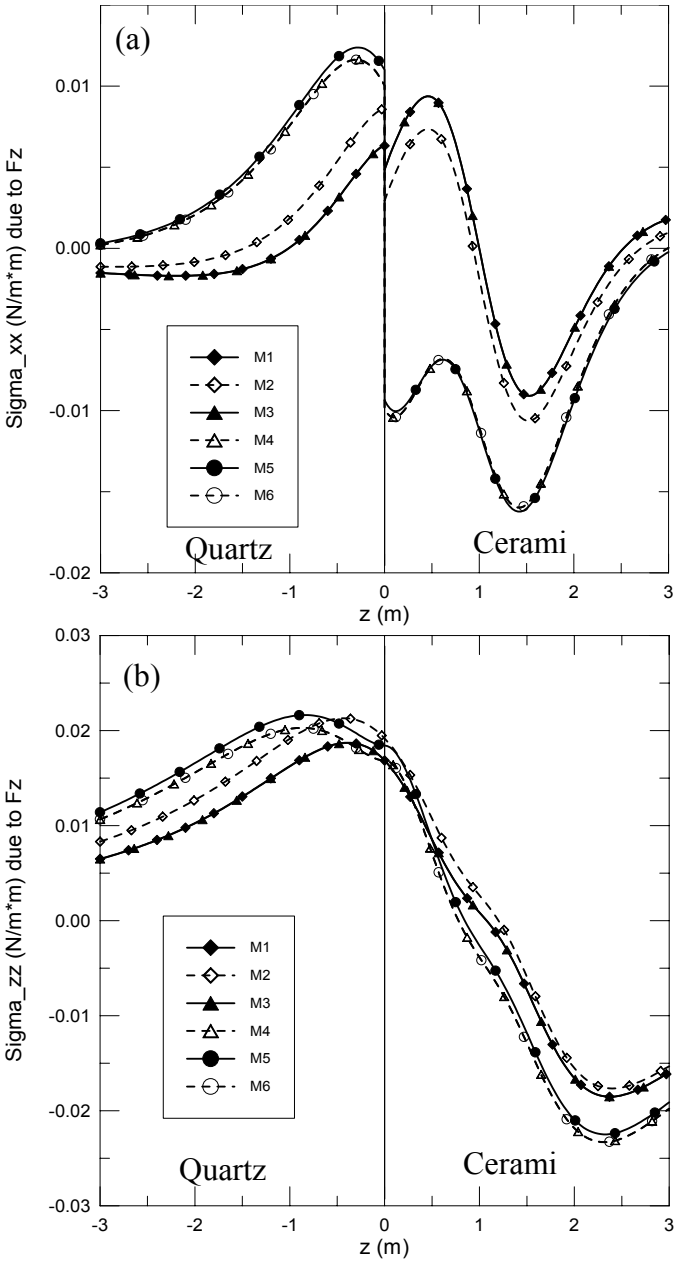
(a)
Sigma_xx (N/m*m) due to Fz
0.01
0.00
-0.01
-0.02
M1
M2
M3
M4
M5
M6
Quartz
Cerami
-3
-2
-1
0
1
2
3
z (m)
(b)
Sigma_zz (N/m*m) due to Fz
0.03
0.02
0.01
0.00
-0.01
-0.02
-0.03
M1
M2
M3
M4
M5
M6
Quartz
Cerami
-3
-2
-1
0
1
2
3
z (m)

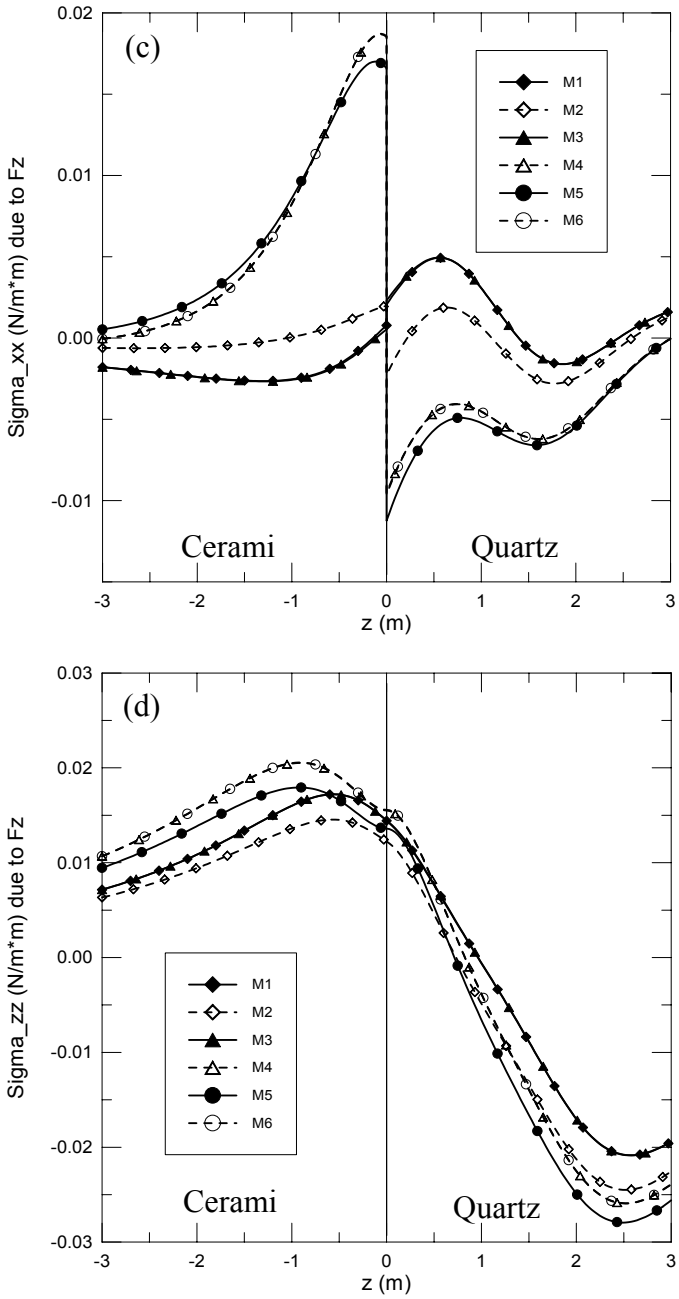

Figure 5. Variations of stress components σ_{xx} and σ_{zz} along vertical line $\boldsymbol{x}$ =(1m,1m,z) in the ceramic/quartz bimaterials (a & b) and quartz/ceramic bimaterials (c & d) due to a

point force of $1N/m^3$ applied at $\boldsymbol{d}$=(0,0,1m) in the z-direction. Curves M1 to M6 correspond to the interface Models 1 to 6, respectively.

7. Conclusions

In this paper, we have derived the 3D Green's functions of point-force and point-charge in anisotropic and piezoelectric bimaterials with six different interface models. By introducing certain modified bimaterial Stroh matrices, along with the extended Stroh formalism and the Mindlin's superposition method, the Green's functions have been expressed in terms of a concise and mathematically similar uniform form. With the exception of the bimaterial Green's function corresponding to the perfect-bond interface Model 1, which was solved previously by Pan and Yuan (2000), the Green's function solutions for other five interface models are solved for the first time. Furthermore, the corresponding 2D Green's functions, in an exact-closed form, for these six different interface models, have been also derived using directly the 3D Stroh matrices at a fixed polar angle.

The effect of different interface conditions on the mechanical and electrical quantities has been also studied and discussed in details. To illustrate the significance of different interface conditions, Green's elastic stresses and electrical displacements are calculated for two bimaterial systems made of two typical piezoelectric materials, namely, the quartz with weak coupling and ceramic with strong coupling. Based on the numerical results, the following new features have been observed:

1). When a mechanical point source is applied, different interface models can produce significant different electrical responses (for both the amplitude and shape) in the strongly coupled ceramic half-space and negligible electrical displacements in the weakly coupling quartz half-space.

2). When an electrical point source is applied, the interface Models 1 and 3 (mechanical perfect-bond), and Models 4 and 6 (mechanical smooth-bond) predict, respectively, nearly identical stresses (components σ_{xx} and σ_{zz}), implying that the normal stress field alone cannot differentiate the electrical open interface condition from the perfect-bond electrical interface condition (i.e., the electrical potential and the normal electrical displacement component are continuous across the interface). Furthermore, when an electrical point source is applied in the strongly coupled ceramic half-space, the responses of the normal stress component σ_{zz} in both half-spaces are roughly divided into two groups: One is related to the interface Models 2 and 5 (electrically closed interface), and the other to the other four interface models.

3). When an electrical point source is applied in the ceramic half-space, the electrical displacements in the quartz half-space are negligible, while those in the ceramic half-space clearly fall into two groups with one corresponding to Models 2 and 5 (electrically closed interface), and the other to the remaining four interface models. If, however, an electrical point source is applied in the quartz half-space, then the distributions of the electrical displacements in the quartz half-space are clearly separated into other two groups: one that corresponds to the interface Models 3 and 6 (electrically open interface), and the other to the other four interface models.

4). When a mechanical point source is applied, the responses of the stresses, in particular, the horizontal normal stress component σ_{xx}, are more or less divided into two groups that are mainly controlled by the mechanical perfect-bond and smooth-bond interface conditions. However, the electrically closed interface condition may disturb the stress distributions.

These coupling features in anisotropic and piezoelectric bimaterials with imperfect interface conditions are new and should be of special interest in the design of piezoelectric composites, in the study of the Eshelby's problem, and in the numerical modeling of strained semiconductor devices based on the bimaterial Green's function method. In particular, to apply the present solutions to the modeling of 2D quantum wire and 3D quantum dot semiconductor structures, a generalized Betti's reciprocal theorem can be employed that connects, in 3D for example, the point-force/point-charge Green's function to the point-eigenstrain (or point quantum dot) Green's function (Pan, 2002b).

Appendix A: 2D Piezoelectric Bimaterial Green's Functions with Imperfect Interfaces

Similar to the 3D bimaterial Green's function studies presented in the main text, we consider an anisotropic and piezoelectric full-space made of two half-spaces with interface at z=0. Again, let us assume that materials 1 and 2 occupy the upper (z>0) and lower (z<0) half-spaces, respectively (Figure 1). Here, however, it is required that the deformation is independent of the y-coordinate (i.e., the generalized plane strain deformation in the (x,z) plane). We further let an extended line force $\boldsymbol{f} = (f_1, f_2, f_3, -q)^t$ and an extended line dislocation (i.e., a Burgers vector) $\boldsymbol{b} = (\Delta u_1, \Delta u_2, \Delta u_3, \Delta\phi)^t$ be applied at (x,z)= (0,d) with d>0 in material 1 (Figure 1). We remark that under the 2D deformation assumption, the bimaterial Green's function for the perfect-bond interface Model 1 can be derived using the one-complex-variable function approach (Suo et al., 1992; Pan, 1999). However, for the more general interface models discussed in this paper, the Stroh formalism is found to be more convenient.

Similar to the purely elastic bimaterial case (Ting, 1996), it can be shown that the analytical bimaterial Green's functions (i.e., the extended displacements and stress functions) can be expressed as

$$\begin{aligned}\boldsymbol{u}^{(1)} &= \frac{1}{\pi}\mathrm{Im}\left\{\boldsymbol{A}^{(1)}\langle \ln(z_*^{(1)} - p_*^{(1)} d)\rangle \boldsymbol{q}^{\infty}\right\} + \frac{1}{\pi}\mathrm{Im}\sum_{J=1}^{4}\left\{\boldsymbol{A}^{(1)}\langle \ln(z_*^{(1)} - \overline{p}_J^{(1)} d)\rangle \boldsymbol{q}_J^{(1)}\right\} \\ \boldsymbol{\psi}^{(1)} &= \frac{1}{\pi}\mathrm{Im}\left\{\boldsymbol{B}^{(1)}\langle \ln(z_*^{(1)} - p_*^{(1)} d)\rangle \boldsymbol{q}^{\infty}\right\} + \frac{1}{\pi}\mathrm{Im}\sum_{J=1}^{4}\left\{\boldsymbol{B}^{(1)}\langle \ln(z_*^{(1)} - \overline{p}_J^{(1)} d)\rangle \boldsymbol{q}_J^{(1)}\right\}\end{aligned} \tag{A1}$$

for z>0 (material 1), and

$$\begin{aligned}\boldsymbol{u}^{(2)} &= \frac{1}{\pi}\mathrm{Im}\sum_{J=1}^{4}\left\{\boldsymbol{A}^{(2)}\langle \ln(z_*^{(2)} - p_J^{(1)} d)\rangle \boldsymbol{q}_J^{(2)}\right\} \\ \boldsymbol{\psi}^{(2)} &= \frac{1}{\pi}\mathrm{Im}\sum_{J=1}^{4}\left\{\boldsymbol{B}^{(2)}\langle \ln(z_*^{(2)} - p_J^{(1)} d)\rangle \boldsymbol{q}_J^{(2)}\right\}\end{aligned} \tag{A2}$$

for z<0 (material 2). In equations (A1) and (A2), $\boldsymbol{\psi}$ is the extended stress function vector related to the elastic stresses and electrical displacements by

$$\sigma_{1J} = -\psi_{J,3} \;\; ; \;\; \sigma_{3J} = \psi_{J,1} \tag{A3}$$

Also in equations (A1) and (A2), Im stands for the imaginary part, and the superscripts (1) and (2) denote, as in the text, the quantities associated with the material 1 and 2, respectively; $p_J^{(\alpha)}$, $\boldsymbol{A}^{(\alpha)}$, and $\boldsymbol{B}^{(\alpha)}$ are the Stroh eigenvalues and matrices, depending only upon the extended stiffness matrix defined by (2.6). It is pointed out that these 2D Stroh quantities can be directly reduced from their 3D counterparts by setting θ=0 (Pan, 2002a), an interesting direct connection between the 2D and 3D Stroh quantities that has not been observed before. Finally in equations (A1) and (A2),

$$\langle \ln(z_*^{(1)} - p_*^{(1)} d) \rangle = diag[\ln(z_1^{(1)} - p_1^{(1)} d), \ln(z_2^{(1)} - p_2^{(1)} d), \ln(z_3^{(1)} - p_3^{(1)} d), \ln(z_4^{(1)} - p_4^{(1)} d)]$$

$$\langle \ln(z_*^{(\alpha)} - \overline{p}_J^{(1)} d) \rangle = diag[\ln(z_1^{(\alpha)} - \overline{p}_J^{(1)} d), \ln(z_2^{(\alpha)} - \overline{p}_J^{(1)} d), \ln(z_3^{(\alpha)} - \overline{p}_J^{(1)} d), \ln(z_4^{(\alpha)} - \overline{p}_J^{(1)} d)]$$

$$(\alpha = 1,2) \tag{A4}$$

with the complex variable $z_J^{(\alpha)}$ being defined by

$$z_J^{(\alpha)} = x + p_J^{(\alpha)} z \tag{A5}$$

It is noted that the first term in equation (A1) corresponds to the full-plane Green's functions (with material properties of material 1) with

$$\boldsymbol{q}^{\infty} = (\boldsymbol{A}^{(1)})^T \boldsymbol{f} + (\boldsymbol{B}^{(1)})^T \boldsymbol{b} \tag{A6}$$

The second term in equation (A1) and the solution in material 2 (equation (A2)) are the complementary parts of the solution with the complex constant vectors $\boldsymbol{q}_J^{(\alpha)}$ (α=1,2; J=1,2,3,4) to be determined. For a perfect-bond interface at z=0, i.e., the interface Model 1, these constants are required to satisfy the following conditions (J=1,2,3,4)

$$\begin{aligned} \boldsymbol{A}^{(1)} \boldsymbol{q}_J^{(1)} + \overline{\boldsymbol{A}}^{(2)} \overline{\boldsymbol{q}}_J^{(2)} &= \overline{\boldsymbol{A}}^{(1)} \boldsymbol{I}_J \overline{\boldsymbol{q}}^{\infty} \\ \boldsymbol{B}^{(1)} \boldsymbol{q}_J^{(1)} + \overline{\boldsymbol{B}}^{(2)} \overline{\boldsymbol{q}}_J^{(2)} &= \overline{\boldsymbol{B}}^{(1)} \boldsymbol{I}_J \overline{\boldsymbol{q}}^{\infty} \end{aligned} \tag{A7}$$

with

$$\begin{aligned} \boldsymbol{I}_1 = diag[1,0,0,0]; \boldsymbol{I}_2 = diag[0,1,0,0] \\ \boldsymbol{I}_3 = diag[0,0,1,0]; \boldsymbol{I}_4 = diag[0,0,0,1] \end{aligned} \tag{A8}$$

Equation (A7) has a similar structure as equations (3.8a,b). Therefore, the solution for the involved complex constants are readily found to be (Ting, 1996)

$$\begin{aligned} \boldsymbol{q}_J^{(1)} &= (\boldsymbol{A}^{(1)})^{-1} (\boldsymbol{M}^{(1)} + \overline{\boldsymbol{M}}^{(2)})^{-1} (\overline{\boldsymbol{M}}^{(2)} - \overline{\boldsymbol{M}}^{(1)}) \overline{\boldsymbol{A}}^{(1)} \boldsymbol{I}_J \overline{\boldsymbol{q}}^{\infty} \\ \boldsymbol{q}_J^{(2)} &= (\boldsymbol{A}^{(2)})^{-1} (\overline{\boldsymbol{M}}^{(1)} + \boldsymbol{M}^{(2)})^{-1} (\boldsymbol{M}^{(1)} + \overline{\boldsymbol{M}}^{(1)}) \boldsymbol{A}^{(1)} \boldsymbol{I}_J \boldsymbol{q}^{\infty} \end{aligned} \tag{A9}$$

where $\boldsymbol{M}^{(\alpha)}$ are the impedance tensors (as defined in equation (3.13)) with the Stroh matrices $\boldsymbol{A}^{(\alpha)}$ and $\boldsymbol{B}^{(\alpha)}$ depending upon the material properties only.

Following the same procedure, the complex constants involved in the bimaterial Green's solutions (A1) and (A2) for the other five interface Models can also be determined. Similar to equation (A9), the solution can be written as

$$\begin{aligned} \boldsymbol{q}_J^{(1)} &= (\hat{\boldsymbol{A}}^{(1)})^{-1} (\hat{\boldsymbol{M}}^{(1)} + \overline{\hat{\boldsymbol{M}}}^{(2)})^{-1} (\overline{\hat{\boldsymbol{M}}}^{(2)} - \overline{\hat{\boldsymbol{M}}}^{(1)}) \overline{\hat{\boldsymbol{A}}}^{(1)} \boldsymbol{I}_J \overline{\boldsymbol{q}}^{\infty} \\ \boldsymbol{q}_J^{(2)} &= (\hat{\boldsymbol{A}}^{(2)})^{-1} (\overline{\hat{\boldsymbol{M}}}^{(1)} + \hat{\boldsymbol{M}}^{(2)})^{-1} (\hat{\boldsymbol{M}}^{(1)} + \overline{\hat{\boldsymbol{M}}}^{(1)}) \hat{\boldsymbol{A}}^{(1)} \boldsymbol{I}_J \boldsymbol{q}^{\infty} \end{aligned} \tag{A10}$$

where $\hat{\boldsymbol{M}}^{(\alpha)}$ (α=1,2) are the modified impedance tensors defined by equation (3.15), and the modified Stroh matrices $\hat{\boldsymbol{A}}^{(\alpha)}$ and $\hat{\boldsymbol{B}}^{(\alpha)}$($\alpha$=1,2) by equations (3.16) to (3.20) for the five imperfect interface Models, with the polar angle θ being fixed at 0. It is obvious that the difference between the 2D and 3D expressions for the modified impedance tensors and Stroh matrices is that for the 2D deformation, they are functions of the extended stiffness matrix only; but for the 3D deformation, they depend also on the Fourier transform variable θ. We further emphasize that, for both the 2D and 3D deformations, the modified Stroh matrices are used only in the process of determining the involved complex constants.

With the bimaterial Green's functions for the extended displacements and stresses being given by equations (A1) and (A2), the effect of different interface conditions on the mechanical and electrical fields can be studied analytically. Furthermore, their derivatives with respect to the field and source points can be analytically carried out and the resulting Green's functions can then be applied to various problems involving bimaterial full-planes with imperfect interfaces. Similar to the corresponding 3D deformation, the 2D bimaterial Green's functions for the five imperfect interface models have not been reported in the literature, and further extension to other imperfect interface models are also possible based upon the same methodology. We further remark that since these 2D bimaterial Green's functions are in exact-closed form, they will be particularly useful in the analysis of strained quantum wire problems (see, i.e., Freund and Gosling, 1995, Gosling and Willis, 1995, and Ru, 2001).

Acknowledgements

About ten years ago, Dr. Vinod Tewary at NIST and Prof. Frank Rizzo organized the first workshop on Green's functions in Boulder, CO. Due to their leadership as well as advocates from many collaborators, Green's function method is now widely recognized in the nation with NSF and NIST as continuous sponsors. It is with this regard that the author would like to dedicate this small piece of Green's function work to Prof. Rizzo for his well-known contributions to the boundary integral equation method and for his constant supports to the Green's function method. The author would also like to acknowledge Dr. Tewary at NIST and many others for their important contributions to Green's function method. Finally, the author received continual encouragements from Prof. Yijun Liu at University of Cincinnati and Prof. Mitsunori Denda at Rutgers University during the preparation of this paper. This work is supported partially by the University of Akron. More detailed information on Green's function method can be found at http://www.ctcms.nist.gov/gf/.

References

Abbudi, M. and Barnett, D. M. (1990): On the existence of interfacial (Stoneley) waves in bonded piezoelectric half-spaces, *Proc. R. Soc. Lond*. A. **429**, 587-611.

Alshits, V. I., Barnett, D. M., Darinskii, A. N. and Lothe, J. (1994): On the existence problem for localized acoustic waves on the interface between two piezocrystals, *Wave Motion*, **20,** 233-244.

Andreev, A. D., Downes, J. R., Faux, D. A. and O'Reilly, E. P. (1999): Strain distribution in quantum dots of arbitrary shape, *J. Appl. Phys*., **86**, 297-305.

Akamatsu, M. and Tanuma, K. (1997): Green's function of anisotropic piezoelectricity, *Proc. R. Soc. Lond*. A. **453**, 473-487.

Bacon, D. J., Barnett, D. M., and Scattergood, R. O. (1978): The anisotropic continuum theory of lattice defects, *Progress in Materials Sci.* **23**, 51-262.

Barnett, D. M. and Lothe, J. (1975): Dislocations and line charges in anisotropic piezoelectric insulators, *Phys. Stat. Sol.* (b), **67**, 105-111.

Benveniste, Y. (1984): The effect of mechanical behavior of composite materials with imperfect contact between the constituents, *Mech. Materials*, **4,** 197-208.

Benveniste, Y. (1999): On the decay of end effects in conduction phenomena: A sandwich strip with imperfect interfaces of low or high conductivity, *J. Appl. Phys.*, **86,** 1273-1279.

Benveniste, Y. and Chen, T. (2001): On the Saint-Venant torsion of composite bars with imperfect interfaces. *Proc. R. Soc. Lond*., A. **457,** 231-255.

Chen, W. Q. (1999): On the application of potential theory in piezoelasticity, *J. Appl. Mech*., **66**, 808-811.

Chen, W. Q., Shioya, T. and Ding, H. J. (1999): The elasto-electric field for a rigid conical punch on a transversely isotropic piezoelectric half-space, *J. Appl. Mech*., **66**, 764-771.

Davi, G. and Milazzo, A. (2002): Stress and electric fields in piezoelectric composite laminates, *Electronic J. Boundary Elements*, Vol. BETEQ 2001, No.1: 43-50.

Davies, J. H. (1998): Elastic and piezoelectric fields around a buried quantum dot: A simple picture, *J. Appl. Phys*., **84**, 1358-1365.

Davies, J. H. (1999): Quantum dots induced by strain from buried and surface stressors, *Appl. Phys*. *Lett*., **75**, 4142-4144.

Davies, J. H. and Larkin I. A. (1994): Theory of potential modulation in lateral surface superlattices, *Phys. Rev. B.*, **49**, 4800-4809.

Denda, M. and Lua, J. (1999): Development of the boundary element method for 2D piezoelectricity, *Composites Part B-Engineering*, **30**, 699-707.

Ding, H. J., Chen, B., Liang, J. (1997): On the Green's functions for two-phase transversely isotropic piezoelectric media, *Int. J. Solids Struct.*, **34**, 3041-3057.

Dundurs, J. and Hetenyi, M. (1965): Transmission of force between two semi-infinite solids, *J. Appl. Mech.*, **32,** 671-674.

Dunn, M. L. and Taya, M. (1993): An analysis of piezoelectric composite materials containing ellipsoidal inhomogeneities, *Proc. R. Soc. Lond*. A. **443**, 265-287.

Dunn, M. L. and Wienecke, H. A. (1999): Half-space Green's functions for transversely isotropic piezoelectric solids, *J. Appl. Mech.*, **66,** 675-679.

Einfeldt, S., Heinke, H., Kirchner, V., and Hommel, D. (2001): Strain relaxation in AlGaN/GaN superlattices grown on GaN, *J. Appl. Phys*., **89**, 2160-2167.

Eshelby, J. D. (1957): The determination of the elastic field of an ellipsoidal inclusion, and related problems, *Proc. R. Soc. Lond*. A. **241**, 376-396.

Fan, H., Sze, K. Y. and Yang, W. (1996): Two-dimensional contact on a piezoelectric half-space, *Int. J. Solids Struct.*, **33**, 1305-1315.

Fang, H. Y., Yang, J. S. and Jiang, Q. (2001): Surface acoustic waves propagating over a rotating piezoelectric half-space, *IEEE Transactions on Ultrasonic Ferroelectrics and Frequency Control*, **48**, 998-1004.

Faux, D. A. and Pearson, G. S. (2000): Green's tensors for anisotropic elasticity: Application to quantum dots, *Phys. Rev. B.* **62**, R4798-R4801.

Faux, D. A., Downes, J. R. and O'Reilly, E. P. (1996): A simple method for calculating strain distribution in quantum-wire structures, *J. Appl. Phys.*, **80**, 2515-2517.

Faux, D. A., Downes, J. R. and O'Reilly, E. P. (1997): Analytic solutions for strain distribution in quantum-wire structures, *J. Appl. Phys.*, **82**, 3754-3762.

Freund, L. B. (2000): The mechanics of electronic materials, *Int. J. Solids Struct.*, **37**, 183-196.

Freund, L. B. and Gosling, T. J. (1995): Critical thickness for growth of strained quantum wires in substrate V-grooves, *Appl. Phys. Lett*., **66**, 2822-2824.

Gharpuray, V. M., Dundurs, J., and Keer, L. M. (1991): A crack terminating at a slipping interface between two materials, *J. Appl. Mech*., **58,** 960-963.

Gosling, T. J. and Willis, J. R. (1994): The energy of arrays of dislocations in an anisotropic half-space, *Phil. Mag.* A. **69**, 65-90.

Gosling, T. J. and Willis, J. R. (1995): Mechanical stability and electronic properties of buried strained quantum wire arrays, *J. Appl. Phys.*, **77**, 5601-5610.

Grundmann, M., Stier, O. and Bimberg, D. (1995): InAs/GaAs pyramidal quantum dots: Strain distribution, optical phonons, and electronic structure, *Phys. Rev. B.* **52**, 11969-11981.

Hashin, Z. (1990): Thermoelastic properties of fiber composites with imperfect interface, *Mech. Materials*, **8,** 333-348.

Hashin, Z. (1991): The spherical inclusion with imperfect interface, *J. Appl. Mech.*, **58,** 444-449.

Hashin, Z. (2001): Thin interphase/imperfect interface in conduction, *J. Appl. Phys.*, **89,** 2261-2267.

Hearne, S. J., Han, J., Lee, S. R., Floro, J. A., Follstaedt, D. M., Chason, E., and Tsong, I. S. T. (2000): Brittle-ductile relaxation kinetics of strained AlGaN/GaN heterostructures, *Appl. Phys. Lett*., **76**, 1534-1536.

Holy, V., Springholz, G., Pinczolits, M., and Bauer, G. (1999): Strain induced vertical and lateral correlations in quantum dot superlattices, *Phys. Rev. lett.*, **83**, 356-359.

Kim, J. S., Yu, P. W., Leem, J. Y., Lee, J. I., Noh, S. K., Kim, J. S., Kim, S. M., Son, J. S., Lee, U. H., Yim, J. S., and Lee, D. (2001): Energy level control for self-assembled InAs quantum dots utilizing a thin AlAs layer, *Appl. Phys. Lett*., **78**, 3247-3249.

Kouris, D. (1993): Stress concentration due to interaction between two imperfectly bonded fibers in a continuous fiber composite, *J. Appl. Mech.*, **60,** 203-206.

Larkin, I. A., Davies, J. H., Long, A. R. and Cusco, R. (1997): Theory of potential modulation in lateral surface superlattices. II. Piezoelectric effect, *Phys. Rev. B.* **56**, 15242-15251.

Lee, H., Johnson, J. A., Speck, J. S., and Petroff, P. M. (2000): Controlled ordering and positioning of InAs self-assembled quantum dots, *J. Vac. Sci. Technol.*, B. **18,** 2193-2196.

Lee, H., Johnson, J. A., He, M. Y., Speck, J. S., and Petroff, P. M. (2001): Strain-engineered self-assembled semiconductor quantum dot lattices, *Appl. Phys. Lett*., **78**, 105-107.

Liu, Y. J. and Fan, H. (2001): On the conventional boundary integral equation formulation for piezoelectric solids with defects or of thin shapes. *Engineering Analysis with Boundary Elements*, **25,** 77-91.

Mindlin, R. D. (1936): Force at a point in the interior of a semi-infinite solid, *Physics*, **7**, 195-202.

Mura, T. (1987): *Micromechanics of Defects in Solids*, Second, Revised Edition, Kluwer Academic Publishers.

Pagano, N. J. and Tandon, G. P. (1990): Modeling of imperfect bonding in fiber reinforced brittle matrix composites. *Mech. Mater.*, **9**, 49-64.

Pan, E. (1999): A BEM analysis of fracture mechanics in 2D anisotropic piezoelectric solids, *Eng. Anal. Bound. Elements*, **23**, 67-76.

Pan, E. (2002a): Mindlin's problem for an anisotropic piezoelectric half space with general boundary conditions, *Proc. R. Soc. Lond*. A. **458,** 181-208.

Pan, E. (2002b): Elastic and piezoelectric fields around a quantum dot: Fully coupled or semi-coupled model, *J. Appl. Phys*., **91,** 3785-3796.

Pan, E. and Tonon, F. (2000): Three-dimensional Green's functions in anisotropic piezoelectric solids, *Int. J. Solids Struct.*, **37**, 943-958.

Pan, E. and Yang, B. (2003): Three-dimensional interfacial Green's functions in anisotropic bimaterials. *Applied Mathematical Modelling,* (in press).

Pan, E. and Yuan, F. G. (2000): Three-dimensional Green's functions in anisotropic piezoelectric bimaterials, *Int. J. Eng. Sci.*, **38**, 1939-1960.

Papas, C. H. (1988): *Theory of Electromagnetic Wave Propagation*, Dover, New York.

Park, S. and Chuang, S. (1998): Piezoelectric effects on electrical and optical properties of wurtzite GaN/AlGaN quantum well lasers, *Appl. Phys. Lett.*, **72**, 3103-3105.

Pearson, G. S. and Faux, D. A. (2000): Analytical solutions for strain in pyramidal quantum dots, *J. Appl. Phys.*, **88**, 730-736.

Reed, J., Gao, G. B., Bochkarev, A., and Morkoc, H. (1994): Si_3N_4/Si/Ge/GaAs metal-insulator-semiconductor structures grown by in situ chemical vapor deposition. *J. Appl. Phys*., **75,** 1826-1828.

Romanov, A. E., Beltz, G. E., Fischer, W. T., Petroff, P. M., and Speck, J. S. (2001): Elastic fields of quantum dots in subsurface layers, *J. Appl. Phys.*, **89**, 4523-4531.

Ru, C. Q. (1998): A circular inclusion with circumferentially inhomogeneous sliding interface in plane elastosatics, *J. Appl. Mech*., **65,** 30-38.

Ru, C. Q. (2001): Two-dimensional Eshelby problem for two bonded piezoelectric half-planes, *Proc. R. Soc. Lond*. A. **467**, 865-883.

Shilkrot, L. E. and Srolovitz, D. J. (1998): Elastic analysis of finite stiffness bimaterial interfaces: Application to dislocation-interface interactions, *Acta Mater*., **46,** 3063-3075.

Shuvalov, A. L. and Gorkunova, A. S. (1999): Cutting-off effect at reflection-transmission of acoustic waves in anisotropic media with sliding-contact interfaces, *Wave Motion*, **30,** 345-365.

Suo, Z., Kuo, C. M., Barnett, D. M. and Willis, J. R. (1992): Fracture mechanics for piezoelectric ceramics, *J. Mech. Phys. Solids*, **40**, 739-765.

Tevaarwerk, E., Rugheimer, P., Castellini, O. M., Keppel, D. G., Utley, S. T., Savage, D. E., Lagally, M. G., and Eriksson, M. A. (2002): Electrically isolated SiGe quantum dots. *Appl. Phys. Lett*., **80,** 4626-4628.

Tiersten, H. F. (1969): *Linear Piezoelectric Plate Vibrations*, Plenum, New York.

Ting, T. C. T. (1996): *Anisotropic Elasticity*, Oxford University Press, Oxford.

Ting, T. C. T. (2000): Recent developments in anisotropic elasticity. *Int. J. Solids and Structures*, **37,** 401-409.

Ting, T. C. T. (2001): The wonderful world of anisotropic elasticity – An exciting theme park to visit. In "*Proc. 4th Pacific International Conference on Aerospace Science and Technology*", pp.1-7.

Volakis, J. L., Chatterjee, A. and Kempel, L. C. (1998): *Finite Element Method for Electromagnetics*, IEEE Press, New York.

Willis, J. R. (1966): Hertzian contact of anisotropic bodies, *J. Mech. Phys. Solids*, **14**, 163-176.

Yang, J. S. and Tiersten, H. F. (1997): Elastic analysis of the transfer of shearing stress from partially electroded piezoelectric actuators to composite plates in cylindrical bending, Smart Materials & Structures, **6**, 333-340.

Yang, Z., Sou, I. K., and Chen, Y. H. (2000): Anisotropic strain in (100) ZnSe epilayers grown on lattice mismatched substrates, *J. Vac. Sci. Technol.*, B. **18,** 2271-2273.

Yeh, N. T., Nee, T. E., Chyi, J. I., Hsu, T. M., and Huang, C. C. (2000): Matrix dependence of strain-induced wavelength shift in self-assembled InAs quantum dot heterostructures, *Appl. Phys. Lett*., **76**, 1567-1569.

Yu, H. Y. (1998): A new dislocation-like model for imperfect interfaces and their effect on load transfer, *Composites Part* A, **29,** 1057-1062.